

Transport complexity in simple porous media

Owen G. Jepps*

Lagrange Fellow, Dipartimento di Matematica, Politecnico di Torino,

Corso Duca degli Abruzzi 24, 10129 Torino, Italy

Lamberto Rondoni[†]

Dipartimento di Matematica and INFM, Politecnico di Torino,

Corso Duca degli Abruzzi 24, 10129 Torino, Italy

(Dated: November 5, 2018)

We examine the transport behaviour of non-interacting particles in a simple channel billiard, at equilibrium and in the presence of an external field. The channel walls are constructed from straight line-segments. We observe a sensitive dependence on the model parameters of the transport properties, which range from sub-diffusive to super-diffusive regimes. In non-equilibrium, we find a transition in the transport behaviour between seemingly-chaotic and (quasi-) periodic behaviour. Our results support the view that normal transport laws do not need chaos, or quenched disorder, to be realized. Furthermore, they motivate some new definitions of complexity, which are relevant for transport phenomena.

PACS numbers: 05.20.-y, 05.60.-k, 05.90.+m, 89.75.-k

I. INTRODUCTION

One of the fundamental aims of statistical mechanics is to shed light upon the relationship between the macroscopic properties of a system and its underlying microscopic behaviour. In formalising such a relationship, conditions of “molecular chaos” are crucial, and are commonly assumed in order to extract physical properties from microscopic models of macroscopic systems (including from molecular dynamics simulations). In fact, various

*Electronic address: jepps@calvino.polito.it

[†]Electronic address: lamberto.rondoni@polito.it

“Chaotic Hypotheses” (CH) are either explicitly or implicitly assumed in the existing literature; for instance Refs.[1, 2] consider the microscopic dynamics as chaotic, in the sense of uniform hyperbolicity, or of positive Kolmogorov-Sinai entropy, and the CH of Gallavotti and Cohen explicitly states:

CH (Gallavotti-Cohen 1995). *A reversible many-particle system in a stationary state can be regarded as a transitive Anosov system for the purpose of computing the macroscopic properties of the system.*

This hypothesis does not mean that particle systems actually are of the Anosov type, as the mathematical definition implies [3], because the Anosov property is invoked only to obtain results on a limited number of quantities: those which characterize the macroscopic state of the system. Therefore, some of the consequences of the CH are expected to apply to systems which are not Anosov, the Gallavotti Cohen Fluctuation Theorem (GCFT) being one of these consequences [1].

The Ergodic Hypothesis (EH) plays a similar role in statistical mechanics. The assumption of ergodicity in equilibrium systems allows one to make a formal association between the thermodynamics of a molecular system and its underlying mechanical properties, despite the fact that ergodicity is notoriously difficult to prove, and in many cases of physical interest it is known to be violated. Therefore, ergodicity is assumed for the purpose of extracting macroscopic data from microscopic models, largely on the basis that thermodynamic data thus generated appear consistent with observations of real physical systems.

At present there is a wide body of results on the applicability of the EH, and theoretical explanations of why it works have been available for quite some time [4, 5]. Differently, the chaotic hypotheses, recently introduced to describe nonequilibrium systems, are not well understood yet, and the question of how much microscopic chaos, and which notion of chaos, is sufficient to explain the observed macroscopic behaviour remains elusive [6]. For instance, recent results indicate that *thermodynamic-like* connections between the microscopic and macroscopic nature of a particle system can be forged for weaker-than-chaotic dynamical systems. In particular, papers such as Refs.[7, 8] show that behaviours which look like normal diffusion and heat conduction can be observed in polygonal billiards, although their dynamics are not chaotic. Indeed, their topological entropy vanishes, which means that nearby orbits do not separate at an exponential rate. Nevertheless, pairs of orbits eventually

separate, with the only exception being pairs of parallel periodic orbits [10]. Consequently, these systems exhibit a certain sensitive dependence on the initial conditions, and their dynamics may appear highly disordered, indistinguishable to the eye from chaotic motions.

Similarly, diffusive behaviour is observed in non-chaotic one dimensional lattices of maps, and in the Ehrenfest wind-tree model [41], with spatial quenched disorder [11, 12]. Furthermore, the GCFT has been verified for an initial diffusive phase, during transport observed in a nonequilibrium version of the periodic Ehrenfest wind-tree model [13], and in a model of a mechanical “pump”, with flat sides [14].

It is, therefore, of interest to explore such non-defocussing systems in greater detail, in order to understand more deeply the nature of transport in non-chaotic particle systems, and to determine its dependence on the geometry of the medium in which transport takes place. In addition to these more fundamental issues, there is also the practical consideration of the study of transport in porous media, as technological developments lead to the production of transport membranes designed ever more precisely on the atomic scale. In systems where the molecular size is of the same order as the pore width, solid-fluid interactions can dominate intermolecular interactions at laboratory temperatures and pressures, to the extent that the contribution from these intermolecular interactions to the overall transport rate can be neglected, and it is sufficient to consider only the solid-fluid interaction [15]. In this respect, the systems studied in this paper resemble transport in microporous membranes at low (but practically relevant) densities, where interactions are rare. However, such porous media lie at the fringes of our understanding, in terms of connecting their microscopic dynamics and their macroscopic properties, so that their applications can be further developed from an improved understanding of these theoretical issues.

In this paper, we consider the mass transport of point particles in a simple two-dimensional polygonal channel, described in section II, consisting of a unit cell that is replicated infinitely in one dimension, and bounded in the other dimension. Despite being arguably the simplest particle system that could be conceived, we observe (in section IV) a surprising array of transport behaviours — while certain properties of the system demonstrate almost trivial behaviour, other properties display an unpredictable richness, which can be expressed through a sensitive dependence of the macroscopic behaviour on the parameters which define the geometry of the boundary.

In our view, the dependence of the mass transport on the geometry of the system charac-

terizes such transport as “*complex*”. Notions of complexity of billiards dynamics, based on symbolic dynamics, are commonly considered, cf. [16, 17], but in the context of the present paper, it seems more appropriate to focus on the complexity of the mass transport as a function of the parameters of the system, rather than the complexity of the dynamics for one given set of parameters. Concerning this aspect, there are various studies which show that noninteracting particle systems, or lattices of maps, have highly irregular dependences of their transport coefficients on the values of the parameters which define them (see, for instance, [18, 19, 20, 21, 22]). These studies concern chaotic dynamical systems, and show that the diffusion coefficient, or the conductivity, can be quite irregular functions of the applied field, of the shape, or of the map’s slope. However, in systems of particles where these irregularities have been observed, their effects do not preclude important transport properties that are well-known in more regular systems. For instance, the irregular behaviour does not necessarily prevent a linear regime, close to equilibrium [23].

In non-chaotic systems of particles, like the ones considered here, the level of irregularity can grow one step further; it can produce discontinuous and, in fact, even *singular* transport coefficients as functions of the geometry of the systems. If this is the case, not only is the behaviour of the single trajectories unpredictable, and the dynamics is “complex” [24], but the overall transport itself becomes largely unpredictable. In other words, in the case of chaotic dynamics, the unpredictability of the fate of a single initial condition is not reflected in the behaviour of an ensemble of initial conditions, while here the behaviour of the ensemble itself — i.e. the object of interest in transport applications — is unpredictable. In fact, slight differences in the manufacturing of porous membranes may result in totally different transport properties. This leads us to the notion of “*transport complexity*”, which will be discussed in section V.

The dependence of the mass transport on the geometry, i.e. of the statistical properties of the dynamics on the parameters defining the system, must be connected with the structure of the ergodic and mixing properties of these systems. The ergodic properties are only known for systems corresponding to various subsets of the parameter space — however, we have no constructive way of explicitly specifying *which* parameter subsets (cf. Ref.[25]). Moreover, the ergodicity alone does not distinguish very finely between different transport behaviours. There are various numerical works on the ergodic, mixing and transport properties of irrational polygons, see, for instance, Refs.[7, 8, 9, 26, 27, 28, 29]. However, the

models are limited in number, the triangular billiards being the most studied models, and many questions concerning them remain open. Our results can be summarized as follows:

- We find that diffusive behaviour is straightforward to obtain, despite the absence of chaos (in the sense of positive Lyapunov exponents), and the absence of quenched disorder.
- In the nonequilibrium case we find that non-chaotic dynamics makes the use of Gaussian thermostats physically inappropriate. Indeed, the existence of a linear regime is not guaranteed in such systems.
- We find a strong dependence of the transport laws on the geometry of the system. This shows that these non-chaotic models of noninteracting particles cannot be considered as proper thermodynamic systems.
- We propose three ways of quantifying the dependence of the transport laws on the geometry of the systems, i.e. their *transport complexity*.

II. SYSTEM DETAILS

Let us begin by recalling the notion of a polygonal billiard.

Definition 1. *Let \mathcal{P} be a bounded domain in the Euclidean plane \mathbb{R}^2 or on the standard torus \mathbf{T}^2 , whose boundary $\partial\mathcal{P}$ consists of a finite number of (straight) line segments. A polygonal billiard is a dynamical system generated by the motion of a point particle with constant unit speed inside \mathcal{P} , and with elastic reflections at the boundary $\partial\mathcal{P}$.*

As usual, elastic reflection means that the angle between the incoming velocity and the normal to $\partial\mathcal{P}$, at the collision point, equals the angle between the outgoing velocity and the same normal. In the general theory of polygonal billiards, \mathcal{P} is not required to be convex or simply connected; the boundary may contain internal walls. If the trajectory hits a corner of \mathcal{P} , in general it does not have a unique continuation, and thus it normally stops there.

In continuous time, the dynamics are represented by a flow $\{S^t\}_{t \in (-\infty, \infty)}$ in the phase space $\mathcal{M} = \mathcal{P} \times \mathbf{T}^1$, where \mathbf{T}^1 is the unit circle of the velocity angles ϑ . Because the dynamics are Hamiltonian, the flow preserves the standard measure $dx dy d\vartheta$ (with $x, y \in \mathbb{R}$ or \mathbf{T}^2 , such that $(x, y) \in \mathcal{P}$). In discrete time, the dynamics are represented by the “billiard map” ϕ , on

the phase space $\Phi = \{(q, v) \in \mathcal{M} : q \in \partial\mathcal{M}, \langle v, n(q) \rangle \geq 0\}$ where $n(q)$ is the inward normal vector to $\partial\mathcal{M}$ at q , and $\langle \cdot, \cdot \rangle$ is the scalar product. Therefore ϕ is the first return map, and the ϕ -invariant measure on Φ induced by $dx dy d\vartheta$ is $\sin \vartheta d\vartheta ds$, if s is the arclength on $\partial\mathcal{P}$. Unfortunately, these standard measures are not necessarily selected by the dynamics, in the sense that different absolutely continuous measures are not necessarily evolved towards them. This weakens considerably the importance of the standard measures in the case of non-ergodic polygons.

Definition 2. *A polygon \mathcal{P} is called rational if the angles between its sides are of the form $\pi m/n$, where m, n are integers. It is called irrational otherwise.*

While polygonal billiards are easily described, their dynamics are extremely difficult to characterise. For instance it is known that rational polygons are not ergodic, and that they possess periodic orbits. But it is not known whether generic irrational polygons have any periodic orbit. On the other hand it is known that irrational polygons whose angles admit a certain superexponentially fast rational approximation are ergodic [25]. In particular the ergodic polygonal billiards are a dense G_δ set [42] in any compact set \mathcal{Q} of polygons with a fixed number of sides, such that the rational polygons with angles with arbitrarily large denominators are dense in \mathcal{Q} [30]. It is not the purpose of this paper to review exhaustively the properties of polygonal billiards, therefore we refer to the cited literature for further details.

The special class of polygons that we consider consists of channels that are periodic in the x direction, but bounded by walls in the y direction, as depicted in Figure 1. The walls consist of straight edges, and are arranged in a saw-tooth configuration such that the top and bottom walls are “in phase”, i.e. the peaks of the lower and upper walls have the same horizontal coordinate. The channel can therefore be represented as an elementary cell (EC), replicated along the x -axis. We denote by h the height of this cell, and set its length to $2\Delta x = 1$ [43]. The heights of the isosceles triangles comprising the “teeth” along the top and bottom cell walls are denoted Δy_t and Δy_b respectively. We also introduce the mean interior channel height d , defined as $d = h - (\Delta y_t + \Delta y_b)/2$, which is equal to the mean height of the pore volume accessible to particles inside the channel. For convenience, we introduce the angles

$$\theta_i = \tan^{-1} \left(\frac{\Delta y_i}{\Delta x_i} \right), \quad \text{for } i = b, t. \quad (1)$$

In this paper we consider a range of values of h , Δy_t , and Δy_b , which can be classified into two groups. First, we consider systems where $\Delta y_t = \Delta y_b$ (and consequently $\theta_t = \theta_b$). In this case, the top and bottom saw-teeth are parallel with one another. Alternatively, we consider systems where Δy_t and Δy_b are unequal, and the saw-tooth walls are not parallel. The choice of $\Delta y_t = 0, \Delta y_b \neq 0$ (or vice versa) is a special case of this last group – in this case, the horizontal top wall induces a vertical symmetry such that the dynamics is isomorphic to a system where both top and bottom saw-teeth have height Δy_b , but where the saw-teeth are Δx out of phase, as in the equilibrium mechanical pump of Ref.[14]. We will therefore consider these walls as an extension of the first group of parallel saw-tooth walls.

The model described so far can be called an *equilibrium* model, because there is no dissipation of energy, due to external forces or otherwise. A *nonequilibrium* model can be constructed introducing the influence of an external field ϵ , that accelerates the particle in the positive x direction, and of a Gaussian thermostat, which balances the effect of the field, dissipating energy in such a way that the speed of the particle becomes a constant of motion. In this case, the particle obeys the equations of motion

$$\left. \begin{aligned} \dot{x} &= p_x & \dot{p}_x &= -\alpha p_x + \epsilon \\ \dot{y} &= p_y & \dot{p}_y &= -\alpha p_y \end{aligned} \right\} \quad \alpha = \epsilon p_x \quad (2)$$

until it reaches the boundary $\partial\mathcal{P}$, where it undergoes a specular reflection, as in the equilibrium case. The effect of the field is to curve the trajectories, making them concave in the direction of the field. In fact the solution of the equations of motion, for the free flight parts of the trajectory are given by:

$$\tan \frac{\vartheta(t)}{2} = \tan \frac{\vartheta_0}{2} e^{-\epsilon t} \quad (3)$$

$$x(t) = x_0 - \frac{1}{\epsilon} \ln \frac{\sin \vartheta(t)}{\sin \vartheta_0} \quad (4)$$

$$y(t) = y_0 - \frac{\vartheta(t) - \vartheta_0}{\epsilon}, \quad (5)$$

which depend on the initial angle ϑ_0 . We note that the boundary of this system is not defocussing, and the external field has a focussing effect, so that the overall dynamics should not be chaotic, although it is not obvious that this is the case for all values of ϵ . When the external field ϵ is set to zero, one recovers the usual equilibrium equations of motion.

The data in this paper were obtained from molecular dynamics simulations of the channel transport system described above. In both the equilibrium and nonequilibrium cases, the momentum and position of the particle are determined from analytic solutions of the equations of motion. Reported values correspond to averages of distinct simulation runs with different initial conditions for the particle. These initial conditions were randomly generated with a uniform spatial distribution, and a “circle” velocity distribution, expressed by a probability density

$$\frac{1}{2\pi} \delta(\rho - 1) d\rho d\vartheta, \quad \text{with velocity } v = \rho(\cos \vartheta, \sin \vartheta) \quad (6)$$

where the speed is $|v| = \rho = 1$.

III. THEORY

Generally, our interest in studying ensemble properties stems from the foundations of statistical mechanics. From a practical viewpoint, when studying a molecular system, we expect that the specific initial microscopic conditions do not alter the thermodynamic properties of a system. That is, we expect an equivalence between the ensemble and time averages of trajectory properties, such that if we were to wait long enough, the average of a property along almost any trajectory would be independent of the initial condition (and equal to the average of the property on the ensemble of initial conditions). Such a phenomenological requirement is incorporated into the theoretical structure of statistical mechanics through the mathematical notion of ergodicity, which can be summarized as follows. Consider a particle system constituted by N classical particles, described by the equations of motion

$$\dot{x} = G(x); \quad x = (\mathbf{q}, \mathbf{p}) \in \mathcal{M} \subset \mathbb{R}^{6N}, \quad (7)$$

where \mathcal{M} is the phase space, and the vector field G contains the forces acting on the system, and the particles interactions. Denote by $S^t x$, $t \in \mathbb{R}$, the solution of (7) with initial condition x . The macroscopic quantity associated with an *observable*, i.e. with a function of phase $\Phi : \Omega \rightarrow \mathbb{R}$, is defined by:

$$\bar{\Phi}(x) = \lim_{T \rightarrow \infty} \frac{1}{T} \int_0^T \Phi(S^t x) dt. \quad (8)$$

in which the time average represents the fact that macroscopic observations occur on time-scales which are very long compared to the microscopic time-scales, so that the measurement

amounts to a long time average. In general, however, computing that limit is not a trivial task at all. The problem is commonly solved by invoking the EH, which states that

$$\bar{\Phi}(x) = \frac{1}{\mu(\Omega)} \int_{\Omega} \Phi(y) d\mu(y) = \langle \Phi \rangle_{\mu} \quad (9)$$

for a suitable measure μ (the *physical measure*), and for μ -almost all $x \in \Omega$. In principle, ergodic theory should identify the cases verifying the EH, and the physical measures μ , but in practice, this is too hard, if not impossible, to do. Nevertheless, there is now a vast literature on the validity of the EH, which can be understood in different ways, but which finds in Khinchin's arguments on the properties of sum variables, the most convincing explanation [4]. In practice, the time average of the functions of physical interest in systems of many particles is reached before a trajectory has explored the whole phase space (which would take too long), because such functions are almost constant, and equal to the ensemble average. Therefore, the finer details of the microscopic dynamics are not particularly important, except for the requirement of some degree of "randomness" (in order to introduce a decay in correlations between particles in the system). However, it is not clear what properties should be imposed on the dynamics in order to obtain sufficient randomness. Consequently, in a system devoid of dynamical chaos, such as that under investigation in this paper, it is of interest to investigate the behaviour of both the individual and ensemble properties of particles (and their trajectories).

From a thermodynamic viewpoint, diffusion is the transport process generated by gradients in the chemical potentials of the different chemical species in multicomponent thermodynamic systems, or of tagged particles moving in a host environment made of (mechanically) identical particles (self diffusion) [31, 32]. More commonly (and often more conveniently), this process is described in terms of Fickian diffusion, relating the mass flux to gradients in local density. Through the fluctuation-dissipation relation (which rests on the EH), the same diffusion properties are also related to the relaxation of local mass-gradient fluctuations at equilibrium, and therefore to the manner in which the positions of particles evolve during equilibrium dynamics, although the response to an external action, and the spontaneous equilibrium fluctuations are rather different phenomena [44]. Fick's first law for diffusion is expressed by [31]:

$$\mathbf{J}(\mathbf{x}) = -D\nabla n(\mathbf{x}) \quad (10)$$

where \mathbf{J} is the mass flow, D is the (Fickian) self diffusion coefficient, n is the number density,

and \mathbf{x} is the position in space. This law, which can be justified in kinetic theory [32], provides the phenomenological basis for the mathematics of diffusion in molecular systems, leading to the second-order PDE

$$\frac{\partial n}{\partial t} = D \frac{\partial^2 n}{\partial x^2}. \quad (11)$$

known as Fick's second law, where t is the time variable. The well-known Gaussian evolution

$$n(x, t) = (4\pi Dt)^{-1/2} e^{-x^2/4Dt} \quad (12)$$

results from an initial delta-function distribution, and the linearity of (11) ensures that the diffusion of a system of molecules can be considered as the evolution of a superposition of Gaussians. In particular, we recover from (12) the linear growth in the mean-square displacement for macroscopic diffusion processes

$$\langle x^2(t) \rangle = \int_{-\infty}^{\infty} x^2 n(x, t) dx = 2Dt. \quad (13)$$

We note that, if $n(x, t)$ is not a slowly-varying function, higher-order corrections may be introduced. The next approximation has the form

$$\frac{\partial n}{\partial t} = D \frac{\partial^2 n}{\partial x^2} + B \frac{\partial^4 n}{\partial x^4}, \quad (14)$$

where B is called the *super Burnett* coefficient. In this case, the diffusion coefficient can still be defined as in (13) — furthermore, the super Burnett coefficient can be determined via the relation

$$\langle x^4(t) \rangle - 3 \langle x^2(t) \rangle^2 = \int_{-\infty}^{\infty} x^4 n(x, t) dx - 3 \left[\int_{-\infty}^{\infty} x^2 n(x, t) dx \right]^2 = 24Bt. \quad (15)$$

As such, the super Burnett coefficient can be seen as a measure of the degree to which transport is diffusive, in the Fickian sense. We note, however, that it has become customary to call *diffusive* any phenomenon displaying a linear relation between the mean square displacement and the time, like (13), even if there are no multicomponents, or any kind of particle systems at hand. In this paper, we do the same. However, we note the key role played by the assumption of a phenomenological law, such as Fick's, in the preceding argument. In general, for a differing phenomenology, one cannot expect the resulting transport processes to remain diffusive in nature. In the absence of intermolecular interactions (or indeed, of other molecules), there is no phenomenological basis for expecting the mass flux to depend on density gradients, and it is therefore of interest to examine the resulting transport.

In characterising the transport law, we consider the behaviour of the displacement as a function of the time t , denoted $s_x(t)$, at equilibrium. In general, we expect an (asymptotic) relation of the form

$$\langle s_x^2(t) \rangle \sim At^\gamma \quad (16)$$

where the coefficient A represents a mobility, and the exponent γ indicates the corresponding transport law. The symbol $\langle \cdot \rangle$ indicates an ensemble average, which in equilibrium systems is universally derived from the equal *a priori* probability assumption, or the EH. In the following we adopt the same assumption, when considering equilibrium systems, although it is not obvious that one should necessarily do so. Similarly, we adopt the language of thermodynamics, and define the following transport properties:

Definition 3. Assume that $\lim_{t \rightarrow \infty} \langle s_x^2(t) \rangle / t^\gamma = A$, for some $A \in (0, \infty)$, then

- i. If the exponent γ equals 1, the transport is called *diffusive*;
- ii. If $\gamma > 1$, the transport is called *super-diffusive* and, in particular, it is called *ballistic* if $\gamma = 2$ (the mean square displacement is proportional to time);
- iii. The transport is called *sub-diffusive* if $\gamma < 1$.

Away from equilibrium, it is less straightforward to distinguish between the various transport laws, as the thermostat imposes an upper limit of linear growth for s_x , even for super-diffusive transport processes. However, for the diffusive process, we expect the diffusion coefficient, estimated from nonequilibrium transport for a given external field of strength ϵ , to converge to a well-defined value in the zero-field limit. To make this explicit, we define the quantity

$$D(\epsilon) = \frac{kT \langle v_x \rangle}{m\epsilon}, \quad (17)$$

for a system of particles of mass m at temperature T (with Boltzmann's constant k), and mean streaming velocity of $\langle v_x \rangle$, as the *finite-field estimate*, at field ϵ , of the (nonequilibrium) diffusion coefficient. The existence of a linear regime guarantees the convergence of $D(\epsilon)$, in the zero-field limit, to a diffusion coefficient D — that is,

$$D = \lim_{\epsilon \rightarrow 0} D(\epsilon) = \frac{kT}{m} \lim_{\epsilon \rightarrow 0} \frac{\langle v_x \rangle}{\epsilon} \quad (18)$$

Thus, for a *diffusive* process, we expect to observe a linear response to the external field. Furthermore, in a thermodynamic system, we expect this diffusion coefficient to be equal

to that describing equilibrium diffusion. For a super-diffusive process, however, we do not expect a linear response, but rather that $D(\epsilon) \rightarrow \infty$ in the zero-field limit. Due to the thermostat, the maximum mean value of v_x is equal to the initial speed of the particle v . For initial velocity set to unity, $D(\epsilon)$ has upper bound of $1/2\epsilon$ (in reduced units) for any ϵ , so that $D(\epsilon)$ can only diverge in the zero-field limit.

IV. RESULTS

In this section we outline the results we have obtained from simulations of the transport of molecules in the saw-tooth channel system described in section II. We examine the equilibrium transport properties in section IV A, and the nonequilibrium transport properties in section IV B. In both cases, we will be interested in the collective, ensemble behaviour of particles in the system, and how this ensemble behaviour relates to the behaviour of individual trajectories.

A. Equilibrium

The ergodic properties of our systems are not obvious, therefore, there seems to be no immediate choice for a probability distribution in phase space, to be used for the ensemble averages. Nevertheless, the uniform probability distribution (Lebesgue or Liouville measure, defined above) is invariant, and one could think that it is appropriate for transport in a membrane which receives particles from a reservoir, inside which the dynamics is chaotic. Therefore, the ensemble averages in this section are all computed assigning equal weight to all regions of phase space.

1. *Parallel walls, collective behaviour*

In Figure 2 we depict the mean-square displacement, as a function of time, for a series of parallel saw-tooth systems ($\Delta y_t = \Delta y_b = \Delta y$), and we examine systems where the ratio $\Delta y/\Delta x$ varies from 0.25 to 3, so that the angle $\theta = \theta_t = \theta_b$ the saw-tooth makes with the horizontal varies from about 0.08π radian ($\approx 14^\circ$) to about 0.4π radians ($\approx 72^\circ$). Each graph shows results for a single value of $\Delta y/\Delta x$, for various pore heights h . For each choice of Δy

(recalling that $\Delta x = 0.5$), we examined pores with heights $h = 1.5\Delta y, 2\Delta y, 2.05\Delta y, 3\Delta y$ and $21\Delta y$. The corresponding interior pore heights are $d = 0.5\Delta y, \Delta y, 1.05\Delta y, 2\Delta y$ and $20\Delta y$. We note that $h = 2\Delta y$ corresponds to the critical pore width, above which the billiard horizon is infinite (i.e. there is no upper bound to the length of possible molecule trajectory segments without boundary collisions). We considered sets of initial conditions ranging from 1000 to 5000 particles. Not surprisingly, given the clearly non-diffusive nature of the transport observed in Figure 2, the corresponding super Burnett coefficients do not appear to have a well-defined value, but diverge over time.

The same data have also been generated for a series of systems with one flat wall and one saw-tooth wall, which always have an infinite horizon. For these systems, we set $\Delta y_t = 0$, and considered the same ratios $\Delta y_b/\Delta x$ as were examined in the parallel saw-tooth systems with pore heights $h = 1.05\Delta y_b, 2.5\Delta y_b$ and $20.5\Delta y_b$ (which have corresponding interior heights $d = 0.55\Delta y, 2\Delta y$ and $20\Delta y$). Sets of initial conditions ranged from 1000 to 5000 particles. There appeared to be a longer initial transient period for the systems with one flat wall, but otherwise the results were qualitatively the same as for the parallel wall, despite the infinite horizon.

Table I shows the values of the exponents obtained from fitting the data in Figure 2 and those for one flat wall to (16), for both the parallel saw-tooth systems and the systems with one flat wall and one parallel wall. In all cases, we observe that the transport is significantly super-diffusive, but *not* ballistic. For the $\Delta y/\Delta x = 1$ system, which is a (parallel) rational polygonal billiard, we observe an exponent $\gamma \approx 1.65$. All other choices of $\Delta y/\Delta x$ represent (parallel) irrational polygonal billiards. For $\Delta y/\Delta x = 1/4$ (where $\theta < \pi/4$), we observe an exponent of $\gamma \approx 1.85$ in all systems. For $\Delta y/\Delta x = 2$ and $\Delta y/\Delta x = 3$ (where $\theta > \pi/4$), we observe a similar exponent in the systems with pore height less than or in the vicinity of $2\Delta y$, and a *reduction* in the transport exponent as the pore height increases. The same value $\gamma \approx 1.85$ has been found by M. Falcioni and A. Vulpiani in the equilibrium version of the periodic Ehrenfest gas of Ref.[13], [33].

We have also examined the distribution of the total x displacements $s_x(t)$, as a function of time. Distributions for the $\Delta y/\Delta x = 1$ system (obtained from 2000 initial conditions) and the $\Delta y/\Delta x = 2$ system (obtained from 5000 initial conditions), obtained at the end of the simulations, are shown in Figure 3. The results for the $\Delta y/\Delta x = 2$ system are typical of the results observed for the other parallel irrational polygonal billiards. Errors are estimated

from the frequency counts used to generate the histograms.

From an initial distribution that is effectively a delta function on the scale of the motion, the transport process produces symmetric distributions, distinct from a Gaussian distribution. For the parallel irrational polygonal billiards, the distribution appears Gaussian out to one standard deviation — however, the distribution at larger displacements is clearly underestimated by the Gaussian. Attempted fits using functions of the form $\exp\{-x^\alpha\}$ fail to capture the shape both at the centre and in the tails, although the tails appear to be well modelled by a distribution of the form $\exp\{-x^{1.4}\}$ (Figure 3a). When $\theta = \pi/4$, however, the distribution bears little resemblance to a Gaussian (Figure 3b). Analogous results in each case were obtained from the systems with one flat wall and one saw-tooth wall.

We have also examined the behaviour of the momenta of particles in our systems. Given that the speed is preserved by the dynamics, the momenta can vary only in orientation, and we therefore examine the effect of the dynamics on the distribution of these orientations. Figure 4 shows the typical behaviour of the distribution of momenta orientations at the beginning, at the midpoint, and at the end of a typical simulation of 5000 particles. We also show a mean distribution obtained from averaging the momentum data over all sampled times, as well as over all trajectories. We find that there are no significant correlations in the distributions of the momenta over the course of the simulation — while the distribution of orientations, as a function of time, does not converge to the uniform distribution over the time-length we have considered (as we might expect it to for a large system of interacting particles), any memory effects do not appear to have a significant influence on the overall distribution at any instant, which remains close to uniform. Again, the same conclusion can be drawn from similar examination of the systems with one flat wall and one saw-tooth wall.

Remark 1. *That the angle of the walls with the horizontal plays a role in the determination of the transport law, while the width of the pores does not appear to do so, is reminiscent of the case of dispersing billiards. There, the infinite horizon adds a logarithmic correction to the dependence of the mean square displacement on time, which is rather hard to detect numerically. Despite the lack of chaos, our non-dispersing billiards could enjoy similar logarithmic corrections when the horizon is infinite. More surprising is the fact that in some cases the transport exponent (not just the matter transport) decreases as the pore width increases while the horizon is finite, and only increases again once the horizon is infinite.*

2. Parallel walls, individual behaviours

From the results we have obtained, there appear to be well-defined collective behaviours that are attributable to the systems we have studied — that is to say, the mean values of the properties obtained from simulation appear to converge, in the limit of a large number of independent trajectories (or particles), to well-defined values. In analogy to what we have presented above, we examine the evolution of the individual particle momenta, and the x displacements.

The picture of the momenta is trivial in the $\Delta y/\Delta x = 1$ systems, because for $\theta = \pi/4$ only four orientations per trajectory at most are possible, as determined by the initial condition. The picture of the momenta for irrational systems is less predictable. Over the course of the simulations, sequences of momenta, *sampled at intervals of 10^4 time units*, were collected. In Figure 5 we show such a sequence of momenta, sampled from a system where $\Delta y/\Delta x = 3$, accumulated up to the 5×10^5 time units (Figure 5a), 2×10^6 time units (Figure 5b), and 10^7 time units (Figure 5c). The momenta are represented by symbols (circles) on the unit circle \mathbf{T}^1 , while the lines indicate the sequence of the sampled momenta. It is clear from Figure 5 that, despite consisting of up to 1000 different sampled momenta, the number of distinct momenta visited by the particle is relatively small (of the order of 10-20). Furthermore, the growth of this set is gradual, and strongly correlated to the set of momenta that precede it in the sequence of momenta visited by the particle. The choice of θ irrationally related to π permits, in principle, the exploration of the whole unit circle of orientations. However, it is clear that the nature of the sequence of wall collisions limits the rate at which such an exploration of the unit circle can be achieved. This slow growth was observed for simulation times up to 10^9 time units (not shown here).

In Figure 6 we show the sequence of the first 1000 momenta, sampled every 10^4 time units, for six distinct initial conditions in a $\Delta y/\Delta x = 3$ system. In each case, the available velocity phase space is gradually explored by the particle. We note that the rate and manner in which this exploration takes place (as indicated by the lines joining consecutive sample momenta) depends significantly, and *unpredictably*, on the initial condition, as is demonstrated by the visibly different structures generated by each. This feature is common to all parallel irrational polygonal billiards examined — for systems with parallel saw-tooth walls and systems with one flat wall and one saw-tooth wall. The flat wall in these latter systems

induces a vertical symmetry that is absent in the parallel systems, and appears to increase the range of momenta visited by particles — however, a similar degree of connectivity is observed in both cases.

Finally, we turn our attention to the behaviour of the displacements $s_x(t)$ for individual initial conditions, as a function of time, which we expect to give further insight into the manner in which the momentum space is explored. In Figure 7, we show $s_x(t)$ as a function of time over four different time-scales for a single particle trajectory in a system where $\Delta y/\Delta x = 0.25$. Again, such a trajectory is typical of the results observed for the parallel irrational polygonal billiards examined. In Figure 8, we show an analogous set of results for transport of a particle in a (rational) $\theta = \pi/4$ system.

In Figure 7a, the dynamics appear somewhat random on the scale of 10^6 time units, although on closer inspection it is clear that certain sections of the trajectory are repeated. Indeed, the occurrence of repeated segments is more obvious in Figure 7b, where after an initial transience of 10^6 steps, the simulation appears to reach a periodic orbit, before changing to another orbit in the interval at about 3.5×10^6 , then reverting to the original orbit at around 8×10^6 time units. On a longer time scale (Figure 7c), the transport appears to alternate between these two almost periodic orbits. However, on the scale of 10^9 time units (Figure 7d), the evolution of s_x takes on quite a different appearance, bearing a similarity with what one might observe for the random motion of a particle in a low-density gas. Such a resemblance suggests that, on this time-scale, there could be sufficient memory loss of the preceding momentum values for the trajectory to appear random. Even at this stage, however, the number of distinct momenta visited by the particle is still limited to the order to 10-100.

In contrast, we recall that the transport behaviour in the $\theta = \pi/4$ system is restricted to a maximum of four distinct momenta, for each initial condition. Despite this apparently strong limitation, a richness in behaviour is still evident. In Figure 8, we observe strongly recurrent behaviour on all time-scales observed, although the nature of the recurrence varies on all observed time-scales, and is likely to continue to do so at larger and larger scales. We note that Figure 7d and Figure 8c represent the evolution of s_x over the same time-length — however, while this evolution appears random in the irrational system, the motion is regular in the rational case. The regularity is less trivial in Figure 8d, with four small steps between the first two large steps, but only three small steps between the second two large

steps, showing that the apparent regularity doesn't make the dynamics easily predictable.

In Figure 9a, we show the distribution of displacements obtained by dividing the 10^9 time-unit trajectory for the $\Delta y/\Delta x = 0.25$ system into segments of shorter time periods, in order to compare with the approximation to the ensemble distribution obtained from averaging over trajectories with independent initial conditions. It is clear from the figure that the two distributions are significantly different — while the ensemble distribution demonstrates the near-Gaussian properties observed earlier, the distribution from the single trajectory is significantly skewed (as could be expected from Figure 7), and has a distribution that is much narrower than that of the ensemble. The correlations observed along the trajectory in Figure 7 lead to a distribution of displacements that is not at all characteristic of the ensemble, up to a time of one billion time units.

In Figure 9b, we show the distribution of displacements obtained by dividing the 10^{10} time-unit trajectory for the $\Delta y/\Delta x = 1$ system into segments, as done above. In contrast with the results for the $\Delta y/\Delta x = 0.25$ system, the distribution obtained in this fashion shows excellent agreement with ensemble distribution of trajectories.

Remark 2. *The overall transport is ultimately slower in the rational systems than in the irrational systems. Furthermore, despite the limitations on the velocities that each single trajectory can take, which differ from trajectory to trajectory, the distributions of displacements exhibited by one rational trajectory equals the distribution of the ensemble, while this is not the case for the irrational trajectories!*

3. Unparallel walls, collective behaviours

We have examined the transport properties of a series of unparallel saw-tooth systems, chosen such that the ratios $\Delta y_b/\Delta x$ lie in the vicinity of the golden ratio. In Figure 10 we show the behaviour of the mean-square displacement, and the estimated diffusion coefficient, as a function of time, for a series of unparallel saw-tooth systems where $\Delta x = 0.5$, $\Delta y_t/\Delta x = 0.62$, and $\Delta y_b/\Delta x = 0.65$. In analogy to the results above, we have examined these systems at the same range of pore heights based on the mean interior pore height $d_c = (\Delta y_t + \Delta y_b)/2$ at which the horizon becomes infinite — at $d = 0.5d_c, d_c, 1.05d_c, 2d_c$ and $20d_c$.

Despite containing data from 10^4 independent initial conditions, the data in Figure 10 exhibit features suggesting that they have not yet converged to a final result. These features

correspond to significant jumps in the mean-squared displacements (and consequently the finite-time estimate of the diffusion coefficient), resulting from short bursts of quasi-periodic behaviour (i.e. ballistic transport). We note from Figure 10 that the effects of the bursts appears to grow as the horizon is opened. Similar jumps are observed in the time-evolution of the super Burnett coefficients, indicating that the bursts contribute to driving the system away from a Gaussian distribution.

To give some sense of the size and frequency of these bursts, we show the distribution of displacements obtained over intervals of 10^5 time units, combining contributions from all 10^4 initial conditions, in Figure 11. We observe excellent agreement with the Gaussian distribution, out to several standard deviations. However, in the tail of the distribution we find a non-negligible contribution from large-scale displacements, to which we attribute the behaviour of the super Burnett coefficients. These contributions correspond to the bursts observed in Figure 10, and it is clear that a huge number of initial conditions would be required before the overall effect of this tail distribution could be realised by simulation.

Table II shows the values of the exponents obtained from fitting the data from the observed systems to (16), and obtain behaviour that is close to diffusive. Errors in the Table were determined using a Marquardt-Levenberg non-linear least squares fit. The significant errors in the data arise from the ballistic bursts, so that a least-squares error estimate, more appropriate for random errors, may not be as appropriate here. However, the least-squares error estimates still provide useful information regarding the relative errors in the data obtained for the various systems.

From Figure 11 it is clear that the bursts only occur for a small number of particles. We have found that, in each case, only 2 or 3 initial conditions are responsible for the ‘significant’ bursts — that is to say, if the contribution from these 2 or 3 particles (in 10000) is neglected, the resultant behaviour is diffusive within statistical error, and the fluctuations all lie within error about this mean diffusive behaviour. Within statistical error, one could conjecture that the effect of these ‘significant’ bursts is not sufficient to drive the behaviour away from diffusive behaviour, given the decay back to diffusive transport observed in Figure 10 after each burst. Clearly, however, it cannot be excluded that the effect of these bursts is to drive the transport at a rate somewhat faster than diffusive, either with an exponent slightly greater than 1, or with some slower correction, such as the $\ln t$ correction for the Sinai billiard. We note, with the Sinai billiard in mind, that the bursts responsible for this

potentially super-diffusive behaviour are observed in systems with both open and closed horizons.

In Figure 12, we show the distribution of displacements after 10^6 time units, and after 10^7 time units, from the trajectories of individual particles, again noting that the initial distribution is effectively a delta function since all particles begin from the same unit cell at $s_x = 0$. Even after 10^6 time units, the distribution of displacements is very well fit by a Gaussian, consistent with our observations of a diffusive transport rate, and in contrast to the results for the parallel walls.

As with the case of parallel walls, the momenta do not appear to be significantly correlated over the course of the simulation, and there is stronger evidence in this case of a convergence to a uniform distribution than in the parallel case.

4. *Unparallel walls, individual behaviours*

As with the parallel systems, we have considered the behaviour along longer individual trajectories, to compare with the ensemble behaviour. For unparallel walls, we find that there is strong agreement between the individual and ensemble behaviours, in terms of the distribution of both the momentum orientations and of the displacements. Sequences of momenta appear random along a trajectory, and the distribution of displacements obtained along a single trajectory demonstrates an excellent Gaussian fit, in agreement with the ensemble results.

B. Nonequilibrium

An alternative method of studying the transport behaviour is to consider the dynamics in the presence of an external field. For thermodynamic fluids, we expect that the transport coefficient determined in the linear response regime (i.e. in the zero-field limit) for the nonequilibrium fluid corresponds to that obtained from the equilibrium fluid properties. It is not clear, *a priori*, that such an equivalence holds for the system examined in this paper, so we examine the nonequilibrium transport properties, as a dynamical system of interest in its own right, as well as to compare its behaviour with that of the equilibrium counterpart.

1. Parallel

For the non-zero-field estimates of the transport coefficient for the $\Delta y = 2$ system, with $d = 0.5\Delta y$, for the four different field strengths $\epsilon = 0.1, 0.01, 10^{-3}, 10^{-4}$, we find that the qualitative behaviour of the particles is highly, and unpredictably, dependent on the field strength. At the highest field, $\epsilon = 0.1$, (Figure 13a) all trajectories have similar qualitative and quantitative properties, demonstrating a “fluid-like” response to the external field — particles are driven in the direction of the field, and the fluctuations about a mean transport rate are small, since the field is strong. At $\epsilon = 0.01$, however, the trajectories exhibit two distinct transport phases — an initial phase where the particle trajectories fluctuate about a mean motion due to the driving field, and a second ballistic phase, where the trajectory finds a periodic orbit (Figure 13b). At this field, two distinct orbits were noted — one consisting of 33 reflections, with period $\tau = 9.6950889\dots$ and mean net speed $v_b \approx 0.31$, the other consisting of 39 reflections, with period $\tau = 12.393386\dots$ and mean net speed of $v_b \approx 0.24$. The orbits are shown in Figure 14. In particular, we note the existence of distinct periodic orbits to which the different trajectories converge, demonstrating that the dynamics at this field strength is *not ergodic*. At lower fields, a transition to periodic orbits is much rarer — however, bursts of almost-periodic orbits are observed, which decay after relatively short times to revert to the previous apparently random behaviour (Figure 13d).

This transition from apparently random transport to ballistic transport has been observed previously in a similar nonequilibrium system with straight walls [13]. There, a transition time was observed between these two transport behaviours, which varied as the inverse square of the external field strength. Our results appear to be consistent with such a relationship, inasmuch as the fraction of observed periodic orbits (indicating ballistic transport) decreases as the field strength increases. We expect that longer simulations would produce a larger fraction of such periodic orbits, and suggest that the reason we do not observe any ballistic transport in the weakest field is due to the much larger time-scale on which such a transition would take place. Unlike the systems in [13], where only the ensemble behaviour was studied, and a smooth transition from diffusive to ballistic transport was observed at finite times, here we consider the single trajectories, and find that their individual transitions are sharp and occur apparently at times not limited by any upper bound.

We show the estimates of $D(\epsilon)$ for the applied fields ϵ for the parallel $\Delta y/\Delta x = 2$ system

in Column 2 of Table III. Over such a range of fields, we would expect to observe either convergence to well-defined value (the diffusion coefficient), or divergent behaviour (bounded by the thermostat). However, we note that $D(\epsilon)$ does not diverge in the zero-field limit, as we would expect for a real fluid which exhibited superdiffusive equilibrium behaviour (such as plug flow).

2. Non-parallel

In contrast to the results for the parallel systems, we find that the individual particle trajectories for the $\Delta y_t/\Delta x = 0.62, \Delta y_b/\Delta x = 0.65, d = 0.5d_c$ system display the same characteristic behaviour for the four different field strengths $\epsilon = 0.1, 0.01, 10^{-3}, 10^{-4}$ examined. Trajectories are typified by an initial apparently random transient behaviour, followed by a transition to ballistic transport in a periodic orbit. The transition time also appears to vary inversely with the field strength. As a consequence, the fraction of trajectories observed to undergo a transition within 10^6 time units decreases with decreasing field, and therefore the lifetime of the non-ballistic regime grows.

For a given field strength ϵ , each ballistic trajectory appears to have the same mean net speed. For each field strength considered, this mean net speed appears to be $v_b \approx 0.48$. We find that the individual trajectories converge to a single periodic orbit that is independent of the initial conditions, but dependent on the field strength. These orbits are shown in Figure 15. We note that these periodic orbits appear to be instances of a continuous family of periodic orbits, converging to a limiting orbit in the zero-field limit. However, this limiting orbit is never observed in the equilibrium trajectories, where it is no longer an attractor.

The existence of a family of attractive periodic orbits, converging to a precise periodic orbit in the zero-field limit, precludes the existence of a linear regime, and is significantly at odds with what one would expect of an ergodic, diffusive system in nonequilibrium. For such systems, we would anticipate the convergence of the nonequilibrium finite-field estimates $D(\epsilon)$ to the equilibrium value D in the zero-field limit. However, the limiting periodic orbit with a finite net speed $v_b \approx 0.48$ implies that the finite-field estimate $D(\epsilon)$ must *diverge* in the zero-field limit.

However, as noted above, the fraction of trajectories that turn ballistic decreases with decreasing field, so that in the $\epsilon \rightarrow 0$ limit we expect this fraction to tend to 0. Further-

more, the behaviour of the trajectories *before* they reach a periodic orbit remains apparently random, and responsive to the field. Consequently, we consider the following approach to constructing the linear regime. At any given time, we neglect those trajectories already captured by a periodic orbit (ie whose transport has become ballistic), and we define a finite diffusion coefficient based upon the remaining trajectories. Usually, one defines the nonequilibrium diffusion coefficient (following the Green-Kubo result (18)) by taking the limits $t \rightarrow 0$ and $\epsilon \rightarrow 0$ separately — here, this is no longer possible if we wish to avoid periodic trajectories, so the limits must be taken simultaneously.

Therefore, given a sufficiently large ensemble of N particles, assume that the fraction $\nu(\epsilon; t)$ of particles which are still in the diffusive regime, at time t and for field strength ϵ , is well-defined. Let $M(N; \epsilon; t)$ be the subset of indices in $\{1, \dots, N\}$ of these still-diffusive trajectories. Assume that for every $\delta > 0$ there is a field $\epsilon_\delta > 0$ such that $\nu(\epsilon; t) \geq 1 - \delta$ if $\epsilon < \epsilon_\delta$ and N is sufficiently large, as seems to be the case in our simulations. For simplicity, assume that there is a function $\epsilon = \epsilon(t; \delta)$, such that $\nu(\epsilon(t; \delta); t) = 1 - \delta/2$. Finally, define $N(\delta) = \lfloor 2l/\delta \rfloor$, where $\lfloor \cdot \rfloor$ represents the integer part, and choose integer l so large that $N(\delta)$ is sufficiently large for the fraction $\delta/2$ to be sufficiently finely realized, for any $\delta > 0$.

Definition 4. *For every $\delta > 0$, distribute at random (with respect to the Lebesgue measure) $N(\delta)$ initial conditions in the phase space. For each of them and for fixed t , consider*

$$D_i(\epsilon; t) = \frac{kT v_{i,x}}{m\epsilon}, \quad i \in \{1, \dots, N\},$$

where $v_{i,x}$ is the mean x -component of the velocity of the i -th trajectory (and other variables defined as in (17)). The nonequilibrium estimate of the diffusion coefficient, if it exists, is defined by

$$\begin{aligned} D_{ne} &= \lim_{\delta \rightarrow 0} \lim_{t \rightarrow \infty} \frac{1}{N(\delta) \nu(\epsilon(t; \delta); t)} \sum_{i \in M(N(\delta); \epsilon; t)} D_i(\epsilon(t; \delta); t) \\ &= \lim_{\delta \rightarrow 0} \lim_{t \rightarrow \infty} \frac{kT}{m\epsilon(t; \delta)} \frac{1}{N(\delta) \nu(\epsilon(t; \delta); t)} \frac{1}{t} \sum_{i \in M(N(\delta); \epsilon; t)} s_{xi}(t), \end{aligned} \tag{19}$$

Thus, for a given choice of δ , and t , we evaluate the estimate of the diffusion coefficient ((17)) considering only those trajectories which have not been captured by a periodic orbit. Then, the limit $t \rightarrow \infty$ includes also the limit $\epsilon \rightarrow 0$, and the limit $\delta \rightarrow 0$ includes the limit $N \rightarrow \infty$. We can now define the following:

Definition 5. *If the equilibrium system has a finite diffusion coefficient D , and $D_{ne} = D$, the system is said to have a linear regime.*

In Table III we report the ‘corrected’ estimates $D(\epsilon)$ for the various fields, where we neglect contributions from ballistic trajectories. In the third column we report estimates for the parallel $\Delta y/\Delta x = 2$ system, and in the fifth column we report estimates for the unparallel $\Delta y_t/\Delta x = 0.62, \Delta y_b/\Delta x = 0.65, d = 0.5d_c$ system. We note that the ‘corrected’ data for the parallel $\Delta y/\Delta x = 2$ system are consistent with a divergent trend (taking into account the large statistical error in the weakest field). For the unparallel system, the equilibrium and nonequilibrium transport properties become more consistent, although they are not conclusively so, because of the large error bars produced by the statistical analysis at low field. Such noise is typical of NEMD simulations at low field, where the signal-to-noise ratio becomes low. Typical NEMD simulations, however, would still converge to yield the same transport coefficient in the long-time limit — in our non-chaotic systems, the transition from random to ballistic behaviour effectively places an upper bound on the time during which random behaviour can be observed. The estimated errors in the diffusion coefficient obtained will therefore depend on the rate at which the mean transition time increases with decreasing field.

Remark 3. *This subsection leads us to conclude that the use of thermostats needs some form of chaos, whether permanent or transient, in order for a linear regime to be observed. This is a cause for concern in the case of thermostatted non-interacting particle systems.*

V. TRANSPORT COMPLEXITY

The properties of the dynamics in these systems are strongly dependent on the values of θ_t and θ_b , and their relative properties — whether they divide one another, and whether they divide π . This sensitivity to the boundary conditions is strongly “unthermodynamic” in nature, and owes its origin to the absence of inter-particle interactions. In real molecular dynamical systems, chaotic behaviour acts as a “double-edged sword” — on the one hand, the sensitivity to initial conditions ensures that trajectories diverge exponentially; on the other hand, under such dynamics almost all trajectories explore the phase space in such a way that they display the same macroscopic behaviour. In the current systems, the dynamics appears to display a sensitivity to initial conditions despite the absence of dynamical chaos. How-

ever, the dynamics is not always sufficiently mixing to cause all trajectories to demonstrate the same average behaviour. By a judicious choice of saw-tooth angles, one can produce dynamics which appear consistent with macroscopic notions of diffusion. Clearly, however, in the absence of intermolecular interactions, one can only expect to describe those aspects of thermodynamics which are based on purely convective processes. Such models lack the essential element of momentum or energy exchange that would be required to describe processes that involve conduction, such as heat transfer or viscous effects, and consequently one cannot draw conclusions on such processes based on the systems of noninteracting particles, such as those examined here.

Similar considerations appear to apply to chaotic noninteracting particle systems, as they also have been found to have thermodynamic properties irregularly dependent on the geometry of the medium [18, 19, 20, 22]. However, in these systems, the presence of chaos induces a higher stability, which is manifested in the fact that the transport coefficient, but not the transport *law*, is affected by the geometry. The transport coefficient, in particular, turns out to be a close-to-continuous function [45], which may, or may not, be a fractal curve, depending on the case. As conceptually interesting as this question is, it does not bear serious consequences for the predicted transport, when the parameters determining the geometry are only known with a finite precision. Indeed, this implies a small error in the transport coefficient, which results in a small uncertainty on the transported quantities. In other words, transport is “predictable” in these systems, hence not “complex”, although the single trajectories may display arbitrarily high complexity (in symbolic dynamics, and information theoretic terms, for instance).

Systems with an unpredictability which affects not only the single trajectories, for fixed geometry, or the transport coefficients, for uncertain geometry, but affects the transport laws themselves, would seem to belong to a class with a higher level of “complexity”. The polygonal channel studied in this paper is such a system. Other map systems with such dependency have also been observed — see Ref.[34] (where the geometry unpredictably gave periodic, diffusive or ballistic behaviour) and Ref.[35]. Our numerical results indicate that the transport law can change from diffusive to sub-diffusive regimes, or alternatively quite high superdiffusive regimes, after small changes of the parameters defining the geometry. To quantify this kind of complexity, we propose the following definitions.

Definition 6. Consider a transport model, whose geometry is determined by the parameter y , which ranges in the interval $[0, h]$, and such that its transport law is given by

$$\lim_{t \rightarrow \infty} \frac{\langle s_x^2(t) \rangle}{t^\gamma} = A, \quad 0 < A < \infty \quad (20)$$

with γ a function of y varying in $[0, 2]$, when y spans $[0, h]$. Let $\Delta\gamma(y_m, y_M) \in [0, \infty]$ be the difference between the largest and the smallest value of γ , for y in the subinterval $(y_m, y_M) \subset [0, h]$, where $\Delta\gamma(y_m, y_M) = \infty$ if in (y_m, y_M) there are points for which (20) is not satisfied by any $\gamma \geq 0$.

i. The transport complexity of first kind of the transport model in (y_m, y_M) is the number

$$\mathcal{C}_1(y_m, y_M) = \frac{h\Delta\gamma(y_m, y_M)}{2(y_M - y_m)} \in [0, \infty) \quad (21)$$

if it exists.

ii. The transport complexity of second kind of the transport model for $y = \hat{y}$ is the exponent $\mathcal{C}_2 = \mathcal{C}_2(\hat{y})$, if it exists, for which the limit

$$\lim_{\varepsilon \rightarrow 0} \frac{\mathcal{C}_1(\hat{y} - \varepsilon, \hat{y} + \varepsilon)}{\varepsilon^{\mathcal{C}_2(\hat{y})}} \quad (22)$$

is finite.

iii. The transport complexity of third kind of the transport model for $y = \hat{y}$ is the limit

$$\mathcal{C}_3(\hat{y}) = \lim_{\varepsilon \rightarrow 0} \Delta\gamma(\hat{y} - \varepsilon, \hat{y} + \varepsilon) \quad (23)$$

These definitions are motivated by the following considerations. If \mathcal{C}_1 does not vanish, the system is surely highly unpredictable from the point of view of transport, in the interval (y_m, y_M) , because its transport law is only known with a given uncertainty. This could be the case, for instance, of a batch of microporous membranes with flat pore walls, whose orientation is obtained with a certain tolerance (transport complexity of first kind). However, \mathcal{C}_1 may diverge around some point of $[0, h]$, as our data seem to indicate, giving rise to an even higher level of transport complexity. Assuming that this divergence has the form of a power law, we take the power as a measure of this second kind of complexity. But even this level of complexity seems to be insufficient for our models, which indicate that $\Delta\gamma(y_m, y_M)$ could be discontinuous. For this reason, we introduce the third kind of transport complexity.

In order to further investigate these notions, and how they relate to our systems, we have considered the transport behaviour in a narrow range about two principal systems, taken from the examples of super-diffusive transport observed in Section IV A. The first principal system is the rational parallel $\Delta y_t/\Delta x = 1$, where we consider the transport behaviour in the limit that $\Delta y_b/\Delta x \rightarrow 1, \Delta y_b/\Delta x > 1$. The second principal is the irrational parallel $\Delta y_t/\Delta x = 2$ system, where we consider the transport behaviour in the limit that $\Delta y_b/\Delta x \rightarrow 2, \Delta y_b/\Delta x > 2$. In Table IV, we show the exponent γ of the transport laws (as per (20)) corresponding to the various choices for Δy_t and Δy_b .

We note that, in both cases, there appears to be a strong discontinuity at $\Delta y_t \Delta y_b$ — when the walls are not parallel, the behaviour is no longer superdiffusive. In the rational case, the transport coefficient appears to depend unpredictably on the Δy_t , but is always distinctly *sub-diffusive*. By contrast, in the irrational case, the transport appears to be essentially diffusive when the walls are not parallel. This behaviour is consistent with that observed in Section IV A 3 for the unparallel walls, which are also irrational.

Due to the discontinuity, the transport complexities \mathcal{C}_1 and \mathcal{C}_2 diverge in these cases, reflecting the high degree of unpredictability that has been observed in the previous sections, which can only be quantified by \mathcal{C}_3 .

VI. CONCLUSION

In this paper, we have examined the transport properties of a dynamical system of remarkable simplicity — a two-dimensional channel with straight-edged walls, populated by non-interacting, point-like particles. Importantly, our choice of system ensures the absence of dynamical chaos. However, this system displays a rich variety of transport behaviours, belying the simplicity of the underlying dynamics.

For the parallel equilibrium systems where the pore angles θ_t and θ_b are equal ($\theta_t = \theta_b = \theta$), we observe super-diffusive (but not ballistic) behaviour. For the parallel irrational polygonal billiards, we find that the root-mean-square displacement grows approximately as $\langle s_x^2(t) \rangle \sim t^{1.85}$ in the equilibrium dynamics. However, for the rational counterpart, $\langle s_x^2(t) \rangle \sim t^{1.65}$ at equilibrium, apparently constrained by the limited range of accessible momenta. These results hold also for the case where $\theta_t = 0, \theta_b = \theta$, which are isomorphic to systems where the top and bottom pore angles are equal, but the saw-teeth are Δx out

of phase. Interestingly, these results are not strongly sensitive to the opening of the horizon (particularly in the case of a shallow saw-tooth angle, $\theta < \pi/4$). It is perhaps surprising that no ballistic motion was observed in these systems, given their simple structure — while the transport is strongly super-diffusive, it is also clearly sub-ballistic in nature.

The behaviour for individual trajectories in these parallel-walled systems are strongly dependent on the initial conditions, in part because of the nature in which the dynamics permits (or rather, restricts) the exploration of the momentum space. This can be understood through the strong correlation of any particular value in the sequence of a particle's momenta with those momenta preceding (and indeed, following) it, developing trajectory sequences through the creation of seemingly quasi-periodic “building blocks” on various length scales. Despite the limitations imposed by this strong correlation, the behaviour of the trajectory over a particular order of magnitude in time is seemingly unpredictable from its behaviour over shorter time-scales, and it appears that the correlation length is of the order of 10^9 time units, or more, when θ is irrational with respect to π , and orders of magnitude longer when θ is rationally related to π . To give some physical sense to this observation, we consider an analogy to the transport of a light symmetric gas molecule (such as methane) along a nanopore of width 1 nm. At room temperature, the unit velocity in our system corresponds to a root-mean-square velocity for methane of approximately 400 m/s, implying that our time units correspond roughly to units of picoseconds. Consequently, the correlation length in the irrational systems is at least of the order of microseconds, during which time the particle will have travelled of the order of millimetres. For the rational systems, the lower bound for the correlation time is closer to the order of seconds, although the mean displacement over this time is of similar order (because of the slower transport, reflected by the smaller value of γ). We note that the mean time between collisions would be much less than this, for all but the most rarified of conditions.

For the nonequilibrium parallel systems, we observe similarly strong dependence on the initial conditions of the trajectories — indeed, at some field strengths we observe clearly non-ergodic behaviour, with the existence of distinct attracting periodic trajectories (with different net speeds) for a single dynamical system. It appears that the existence of periodic orbits is determined by the field strength, although bursts of quasi-periodic behaviour are observed over short time intervals. There is no clear relation between the onset time for ballistic (periodic) transport and the field strength. More fundamentally, there does not

appear to be any clear connection between the non-zero-field estimates of the diffusion coefficient and the zero-field (equilibrium) value (which is infinite in the case of parallel walls). Certainly, there is no evident divergence of $D(\epsilon)$ in the zero-field limit, as one would expect for a super-diffusive thermodynamic system (such as plug flow). Although, these systems could have a diffusion coefficient defined as in section IV, the existence of a linear regime has not been clearly established, because the equality between D and D_{ne} is not guaranteed by our calculations.

For the unparallel systems, where $\theta_t \neq \theta_b$, we observed diffusive transport in the equilibrium system — $\langle s_x^2(t) \rangle \sim t$, with a Gaussian distribution of displacements s_x consistent with the behaviour predicted by (12). The trajectories were more sensitive to the opening of the horizon than for the parallel systems, with occasional short-lived bursts of much faster transport. In contrast to the unexpected richness in behaviour of the parallel systems, in the unparallel systems, the properties of individual trajectories consistently matched ensemble properties. This was also true of the nonequilibrium results, where there was a much clearer field-dependence of the transport behaviour, and in particular the transition to a periodic orbit. In the unparallel systems, the periodic orbit was unique for a given field (and appeared to be continuously dependent on the field), and the mean onset time of the periodic orbit grew with decreasing field strength. This is consistent with the results of Ref. [13], which, however, were obtained for a system with *parallel* boundary walls. However, the wall angles were chosen such that $\tan \theta$ was close to the golden ratio $(\sqrt{5}+1)/2 = 1.618\dots$, so as to “maximise” the irrationality of the relationship of θ to π . It is possible that such a choice leads to much smaller correlation times in the momentum sequence for particle trajectories, and consequently faster convergence to the longer time-scale behaviour more reminiscent of intermolecular collisions, observed in Figure 7.

Despite the apparently ergodic behaviour, however, our results are not conclusive regarding the connection between the equilibrium and nonequilibrium transport behaviours: the existence of a linear response regime, where the non-zero-field estimates $D(\epsilon)$ converge to the equilibrium diffusion coefficient in the zero-field limit is not clear.

Among the systems we have observed, we find that:

- systems with irrational walls are super-diffusive if parallel, but diffusive if rationally related;

- systems with one rational wall and one irrational wall are sub-diffusive;
- systems with two rational walls are super-diffusive.

Furthermore, we identify a means of quantitatively estimating the uncertainty related to the system transport, through the parameters used to define the geometry. Such notions of transport complexity are useful in distinguishing between various transport systems, the range of transport properties that they exhibit, and in particular the predictability of these transport properties. The various transport properties observed in the systems examined in this paper, and their strongly unpredictable nature, are reflected in the divergent values for the proposed transport complexities \mathcal{C}_1 and \mathcal{C}_2 , and in the finite value of \mathcal{C}_3 . We note that, for the sake of simplicity, we have focussed on the dependence of the transport law on just one parameter, but our investigation reveals that transport in our models may depend in a counterintuitive and irregular fashion on other parameters as well, such as h . Striking is the case in which a growth of h implies a reduction of the transport exponent. More complicated notions of transport complexity may then be envisaged, but the conceptual picture outlined here would not change.

This analysis leads us to the following observation. As is well known, the thermodynamical properties of a macroscopic system are not a function of the boundary of the medium; the properties of a fluid, such as its viscosity, do not depend on the geometry of its container, and, in general, the nature of transport is essentially independent of the geometry. Fermi expressed this concept, at the beginning of his book on thermodynamics [36], in which he states: *“The geometry of our system is obviously characterized not only by its volume, but also its shape. However, most thermodynamical properties are largely independent of the shape, and, therefore, the volume is the only geometrical datum that is ordinarily given. It is only in the cases for which the ratio of surface to volume is very large (for example, a finely grained substance) that the surface must be considered.* This is clearly understood in the terms of kinetic theory, which leads to explicit expressions for the mutual or self diffusion coefficients in terms of only the mean-free paths λ for collisions among particles, without any reference to the shape of the containers. Only in the case that λ is of the same order of the characteristic lengths of the container, does this play a role; but in that case, the standard laws of thermodynamics cease to hold, and are replaced by those of highly rarefied gases, or Knudsen gases [31, 37, 38]. Because our systems do not have this extreme ratio of surface

to volume, our results indicate that our systems cannot be considered as thermodynamic systems, much as they remain highly interesting from both theoretical and technological standpoints. Indeed, as has been noted elsewhere [39, 40], much care must be taken in the thermodynamic interpretation of the collective behaviour of systems of non-interacting particles. The arguments of Refs.[39, 40] mainly referred to nonequilibrium systems: here we provide some examples which show that they apply to equilibrium systems as well. All this can be summarized stating that a certain degree of *chaos*, or of *randomness* is required in the microscopic dynamics of particle systems, for them to look like thermodynamic systems, but there are two ways in which this can be achieved. If the randomness is intrinsic to the fluid, the geometry of the system is a secondary issue, and the fluid behaves as a proper thermodynamic system. If the randomness is produced by the geometry of the outer environment, the geometry plays an obviously important role, and systems such as ours do not behave like proper thermodynamic systems.

VII. ACKNOWLEDGEMENTS

We would like to thank R. Artuso, M. Falcioni, R. Klages and A. Vulpiani for helpful feedback from preliminary drafts. We would also like to thank the ISI Foundation for financial support throughout this work.

-
- [1] G. Gallavotti and E.G.D. Cohen. Dynamical ensembles in stationary states. *Journal of Statistical Physics*, 80(5/6):931, 1995.
 - [2] P. Gaspard. *Chaos, scattering and statistical mechanics*. Cambridge University Press, Cambridge, 1998.
 - [3] D. Ruelle. *Elements of differentiable dynamics and bifurcation theory*. Academic Press, Boston, 1989.
 - [4] A.I. Khinchin. *Mathematical foundations of statistical mechanics*. Dover Publications, New York, 1949.
 - [5] G. Gallavotti. *Statistical mechanics, a short treatise*. Springer-Verlag, Berlin, 1999.
 - [6] D.J. Evans, D.J. Searles, and L. Rondoni. Application of the gallavotti-cohen fluctuation

- relation to thermostated steady states near equilibrium. *Physical Review E*, a(b):c, d 2005.
- [7] B. Li, G. Casati, and J. Wang. Heat conductivity in linear mixing systems. *Physical Review E*, 67:021204, 2003.
 - [8] D. Alonso, A. Ruiz, and I. de Vega. Transport in polygonal billiards. *Physica D*, 187:184, 2004.
 - [9] E. Gutkin Billiards in polygons *Physica D* 19:311, 1986.
 - [10] G. Galerpin, T. Krüger, and S. Troubetzkoy. Local instability of orbits in polygonal and polyhedral billiards. *Communications in Mathematical Physics*, 169:463, 1995.
 - [11] F. Cecconi, D. Castillo-Negrete, M. Falcioni, and A. Vulpiani. The origin of diffusion: the case of non-chaotic systems. *Physica D*, 180:129, 2003.
 - [12] C.P. Dettmann, E.G.D. Cohen, and H. van Beijeren. Microscopic chaos from brownian motion? *Nature*, 401:875, 1999.
 - [13] S. Lepri, L. Rondoni, and G. Benettin. The Gallavotti-Cohen fluctuation theorem for a nonchaotic model. *Journal of Statistical Physics*, 99:857, 2000.
 - [14] G. Benettin and L. Rondoni. A new model for the transport of particles in a thermostated system. *Mathematical Physics Electronic Journal*, 7:1, 2001.
 - [15] Owen G. Jepps, Suresh K. Bhatia, and Debra J. Searles. Wall mediated transport in confined spaces : Exact theory. *Physical Review Letters*, 91:126102, 2003.
 - [16] S. Troubetzkoy. Complexity lower bounds for polygonal billiards. *Chaos*, 8(1):242, 1998.
 - [17] E. Gutkin and S. Tabachnikov. Complexity of piecewise convex transformations, with applications to polygonal billiards. *arXiv:math.DS/0412335*, 2004.
 - [18] J. Lloyd, M. Niemeyer, L. Rondoni, and G.P. Morriss. The nonequilibrium Lorentz gas. *Chaos*, 5(3):536, 1995.
 - [19] T. Harayama, R. Klages, and P. Gaspard. Deterministic diffusion in flower shape billiards. *Physical Review E*, 66:026211, 2002.
 - [20] Z. Koza. Fractal dimension of transport coefficients in a deterministic dynamical system. *Journal of Physics A*, 2004.
 - [21] R. Klages and J. R. Dorfman. Simple maps with fractal diffusion coefficients. *Physical Review E*, 74:387–390, 1995.
 - [22] R. Klages and Ch. Dellago. Density-dependent diffusion in the periodic Lorentz gas. *Journal of Statistical Physics*, 101:145–159, 2000.

- [23] N.I. Chernov, G.L. Eyink, J.L. Lebowitz, and Ya. G. Sinai. Steady state electric conductivity in the periodic Lorentz gas. *Communications in Mathematical Physics*, 154:569, 1993 ; N. I. Chernov, G. L. Eylink, J. L. Lebowitz, and Ya. G. Sinai. Derivation of ohm’s law in a deterministic mechanical model. *Physical Review Letters*, 70:2209–2212, 1993 ; N. Chernov. Sinai billiards under small external forces. *Annales Henri Poincaré*, 2:197–236, 2001.
- [24] G. Boffetta, M. Cencini, M. Falcioni, and A. Vulpiani. Predictability: a way to characterize complexity. *Physics Reports*, 356(6):367, 2002.
- [25] E. Gutkin. Billiard dynamics: a survey with the emphasis on open problems. *Regular and chaotic dynamics*, 8(1):1, 2003.
- [26] R. Artuso, G. Casati, and I. Guarneri. Numerical study on ergodic properties of triangular billiards. *Physical Review E*, 55:6384, 1997.
- [27] G. Casati and T. Prosen. Mixing properties of triangular billiards. *Physical Review Letters*, 83:4729, 1999.
- [28] R. Artuso and G. Cristadoro. Weak chaos and anomalous transport: a deterministic approach. *Communications in Nonlinear Science and Numerical Simulations*, 8:137, 2003.
- [29] Roberto Artuso. Anomalous diffusion in classical dynamical systems. *Physics Reports*, 290:37–47, 1997.
- [30] E. Gutkin. Billiards in polygons: survey of recent results. *Journal of Statistical Physics*, 83(1/2):7, 1996.
- [31] S.R. de Groot and P. Mazur. *Non-equilibrium thermodynamics*. Dover Publications,inc., New York, 1984.
- [32] S. Chapman and T.G. Cowling. *The mathematical theory of non-uniform gases*. Cambridge Univ. Press, Cambridge, 1970.
- [33] M. Falcioni and A. Vulpiani. private communication. 2004.
- [34] N. Korabel and R. Klages. Fractal structures of normal and anomalous diffusion in nonlinear nonhyperbolic dynamical systems. *Physical Review Letters*, 89:214102, 2002.
- [35] Edward Ott. *Chaos in dynamical systems*. Cambridge University Press, 1993.
- [36] E. Fermi. *Thermodynamics*. Dover Publications inc., New York, 1956.
- [37] L.E. Reichl. *A modern course in statistical physics*. University of Texas Press, Austin, 1984.
- [38] C. Kittel and H. Kroemer. *Thermal physics*. Freeman & Company, San Francisco, 1980.
- [39] E.G.D. Cohen and L. Rondoni. Particles, maps and irreversible thermodynamics. *Physica A*,

306:117, 2002.

- [40] L. Rondoni and E.G.D. Cohen. On some derivations of irreversible thermodynamics from dynamical systems theory. *Physica D*, 168-169:341, 2002.
- [41] This is one kind of polygonal billiard, with one point particle which moves in the two dimensional plane, and undergoes elastic collisions with scatterers which have flat sides. Such collisions do not defocus neighbouring trajectories, hence chaos is absent.
- [42] A subset Y of a compact metric space X is a dense G_δ set of X , if Y is a countable intersection of dense open subsets of X .
- [43] A simple mirror symmetry operation allows the equilibrium dynamics of the billiard, defined above, to be reduced to an even simpler fundamental domain than the EC, which is only half of the EC. However, the nonequilibrium dynamics which will be considered later, is made of curved trajectories, whose convexity has a precise sign, and is not preserved by the mirror symmetry. Therefore, we do not reduce further the EC.
- [44] For instance, the spontaneous fluctuations around equilibrium states do not dissipate any energy. Indeed, they do not change the state of the system, and continue forever. Differently, the response to an external action dissipates part of the energy received, and may modify the state of the system, or maintain a nonequilibrium steady state.
- [45] while the function may not be continuous, it can be represented by a function $D(\xi) + \epsilon(\xi)$ for geometry parameter ξ , where $\max |\epsilon(\xi)|$ is of the same (if not smaller) order than the errors in measurement, or where $\max |\epsilon(\xi)|/(\partial D/\partial \xi)$ is very small compared to the range of ξ of interest, or both.

Figures

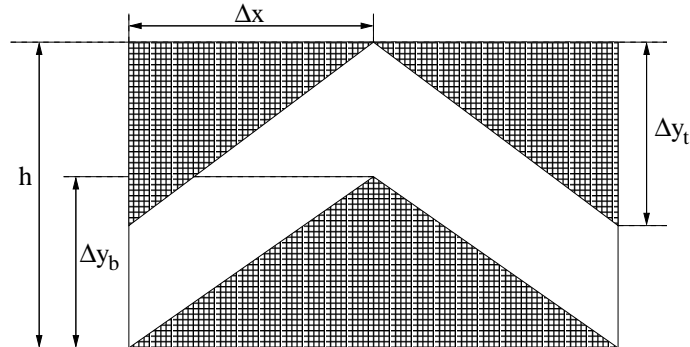


FIG. 1: Symmetric saw-tooth pore model used throughout this paper. The total pore height is denoted h , the width of the repeated unit cell is $2\Delta x = 1$. The “tooth” heights on the top and bottom are, denoted Δy_t and Δy_b respectively.

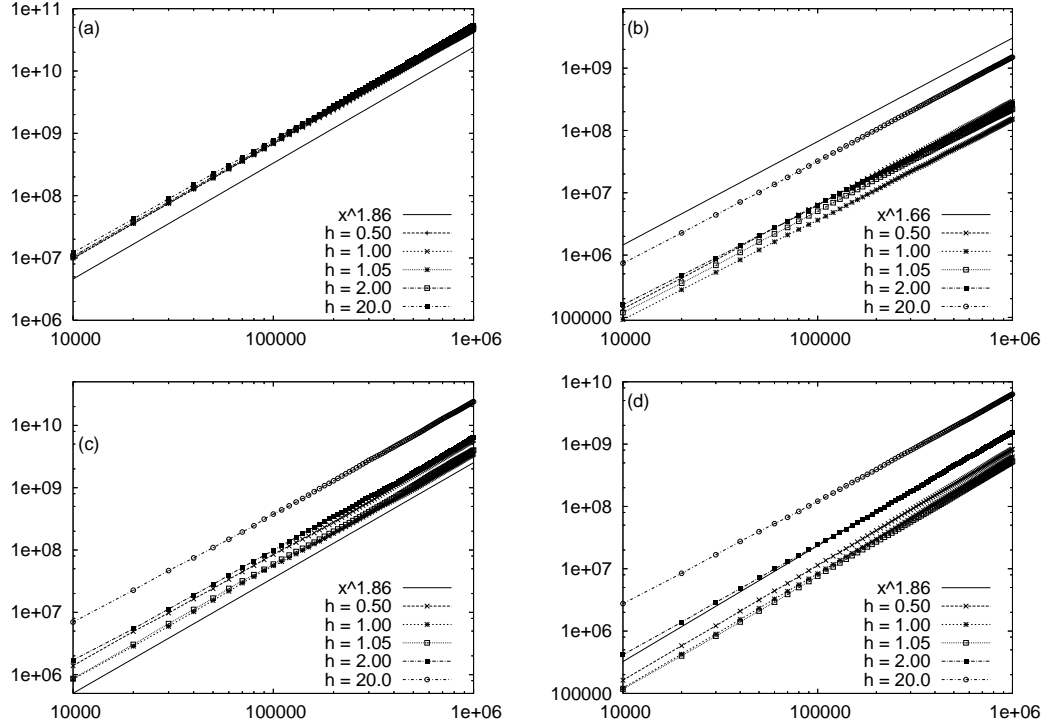


FIG. 2: Evolution of mean-squared displacement for parallel saw-tooth systems, for (a) $\Delta y/\Delta x = 0.25$, (b) 1, (c) 2, and (d) 3. The data are obtained from 1000-5000 initial conditions, and the average number of collisions is of the same order as the total time.

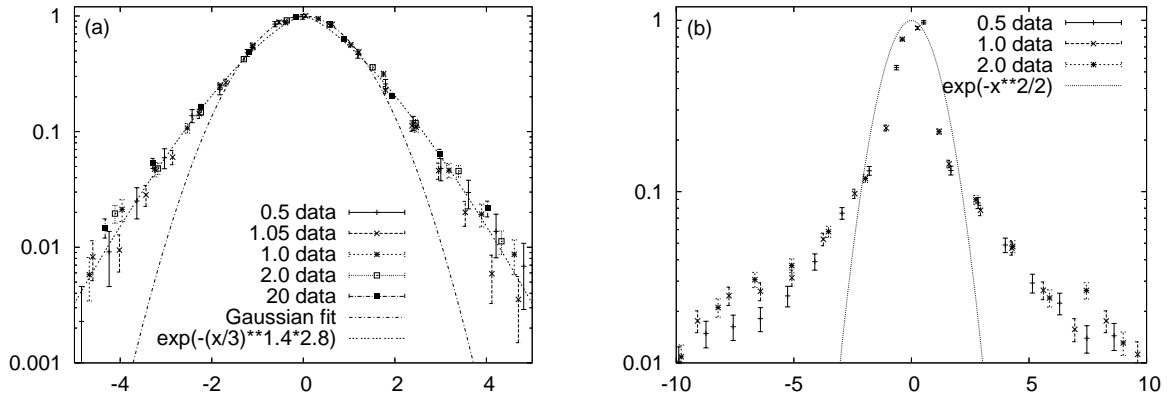


FIG. 3: Distribution of displacements after 10^6 time units for parallel saw-tooth systems, where (a) $\Delta y/\Delta x = 2$, from 2000 initial conditions, and (b) $\Delta y/\Delta x = 1$, from 5000 initial conditions.

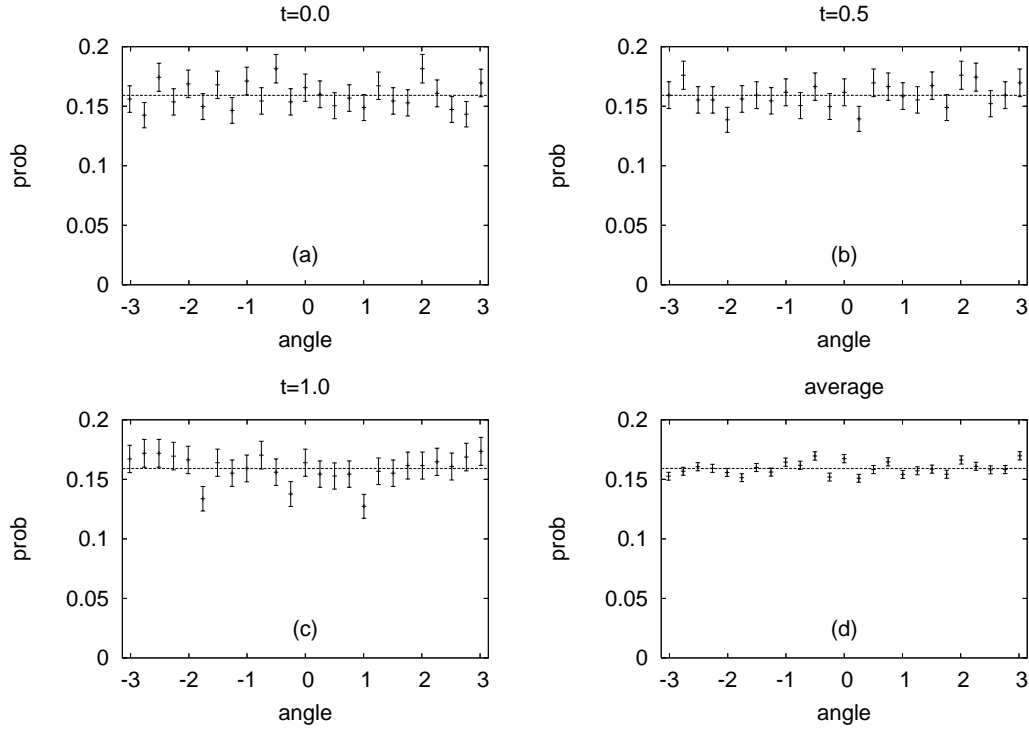


FIG. 4: Distribution of momenta orientations (a) at $t = 0$, (b) at $t = 5 \times 10^5$, (c) at $t = 10^6$, and (d) averaged over all times, for the $\Delta y/\Delta x = 1$ system with $d = 0.5\Delta y$. The dotted line indicates the uniform distribution. Errors are estimated from the frequency counts used to generate the histograms (and are hence smaller in (d), where the data is comprised of more samples).

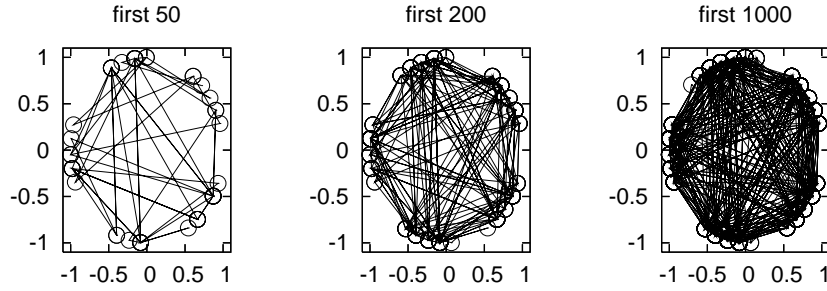


FIG. 5: Momentum progression for a single trajectory up to (a) $t = 5 \times 10^5$ (50 samples), (b) $t = 2 \times 10^6$ (200 samples), and (c) $t = 10^7$ (1000 samples), for the $\Delta y/\Delta x = 3$ system with $d = 2\Delta y$.

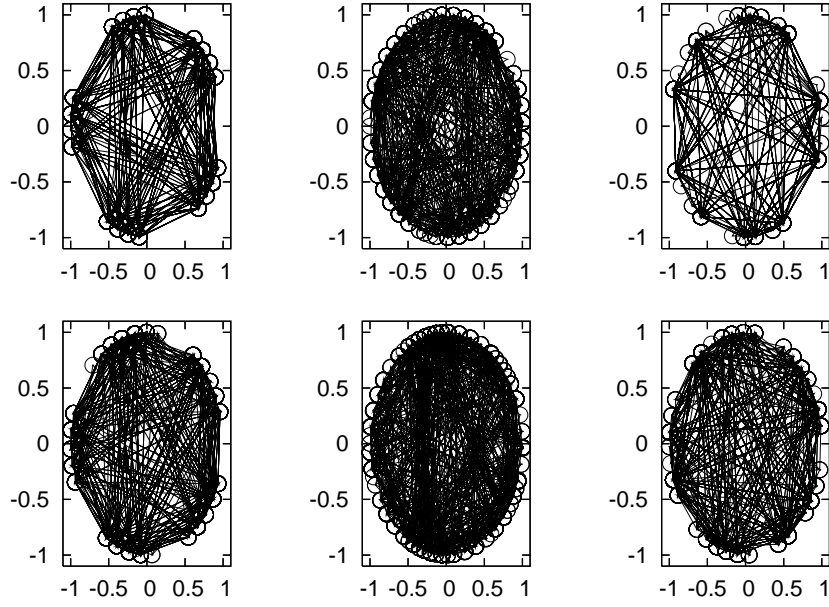


FIG. 6: Sequences of sampled momenta for six different initial conditions, up to 10^7 time units (1000 samples), for the $\Delta y/\Delta x = 3$ system with $d = 2\Delta y$.

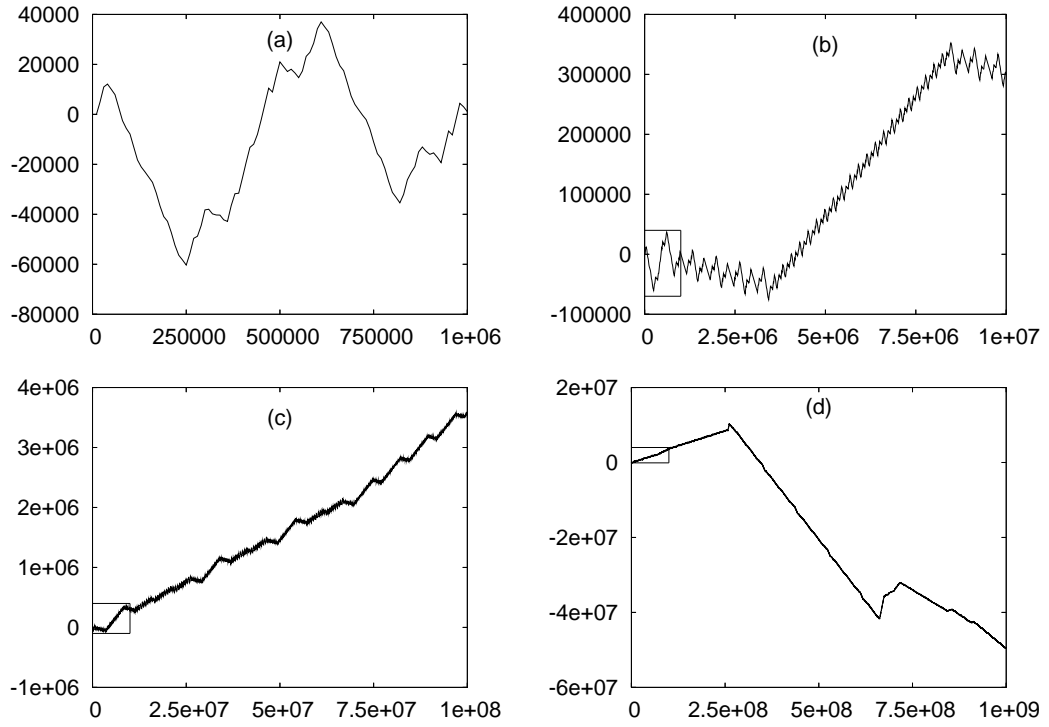


FIG. 7: Example of the time evolution of a particle displacement for the $\Delta y/\Delta x = 0.25$ system ($d = 0.5\Delta y$), for a sequence of four different time-scales. Boxes indicate the position of the previous graph in the sequence.

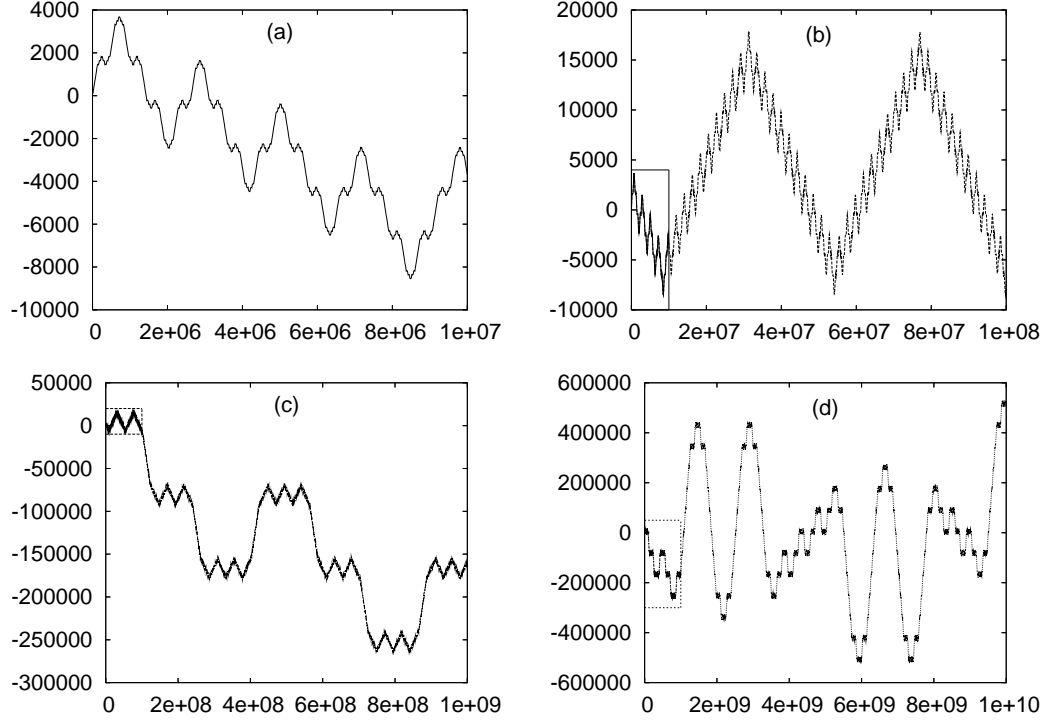


FIG. 8: Example of the time evolution of a particle displacement for the $\Delta y/\Delta x = 1$ system ($d = 2\Delta y$), for a sequence of four different time-scales. Boxes indicate the position of the previous graph in the sequence.

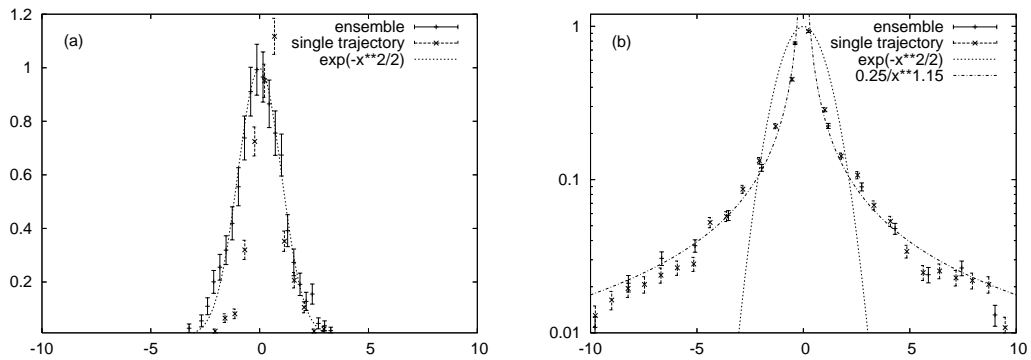


FIG. 9: Histogram of displacements collected along a single trajectory, and from the ensemble of trajectories, for the (a) $\Delta y/\Delta x = 0.25$ ($d = 0.5\Delta y$), and (b) $\Delta y/\Delta x = 1$ ($d = 2.0\Delta y$) systems.

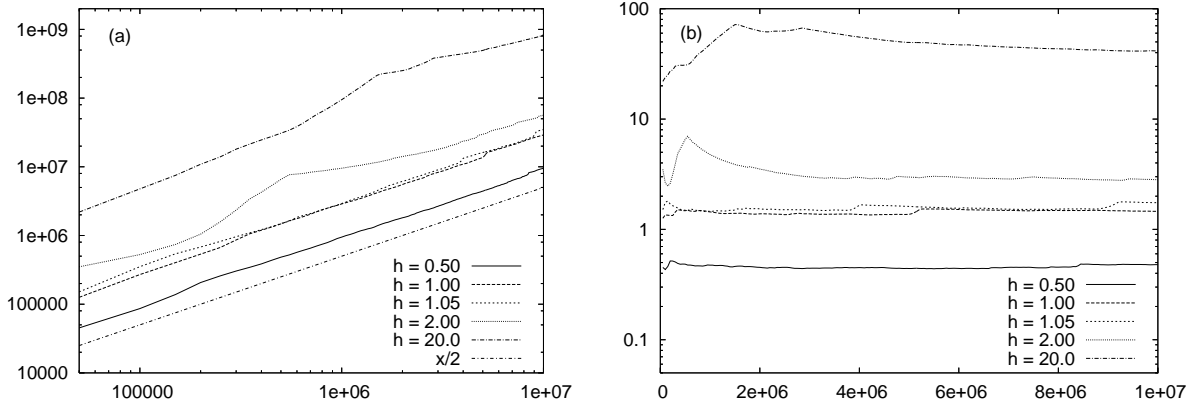


FIG. 10: Evolution of (a) the mean-squared displacement, and (b) the diffusion coefficient, for transport in systems with unparallel saw-tooth walls — $\Delta y_t/\Delta x = 0.62$, $\Delta y_b/\Delta x = 0.65$, $d = 0.5d_c, d_c, 1.05d_c, 2d_c$ and $20d_c$.

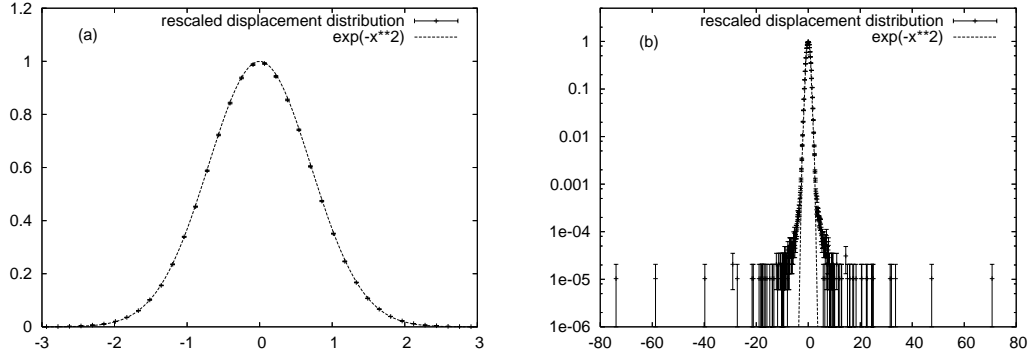


FIG. 11: Displacements over intervals of 10^5 time units, combining contributions from all 10^4 initial conditions, for transport in the system $\Delta y_t/\Delta x = 0.62$, $\Delta y_b/\Delta x = 0.65$, for $d = 0.5d_c, d_c, 1.05d_c, 2d_c$ and $20d_c$: (a) within three standard deviations; and (b) over the full range of displacements (shown using a log-linear plot).

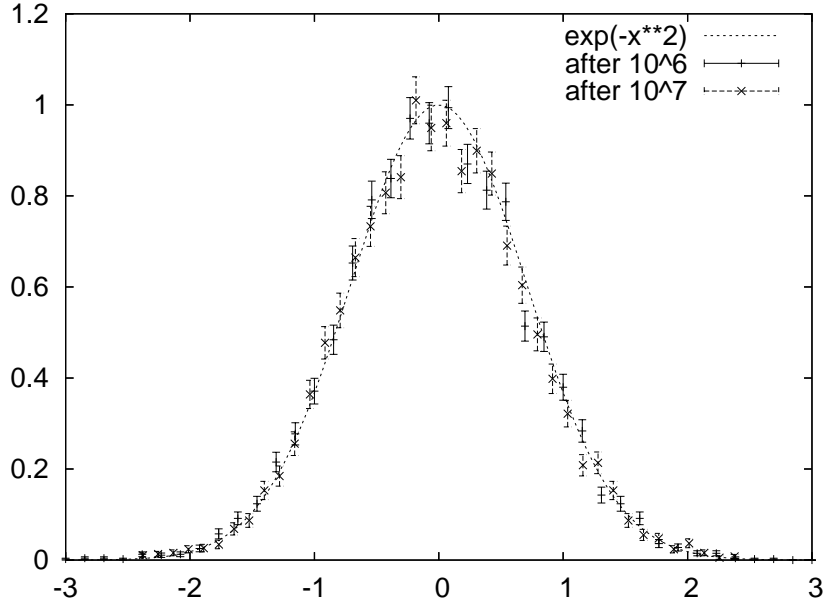


FIG. 12: Distribution of final displacements for unparallel saw-tooth systems where $\Delta y_t/\Delta x = 0.62$, $\Delta y_b/\Delta x = 0.65$, $d = 0.5d_c$.

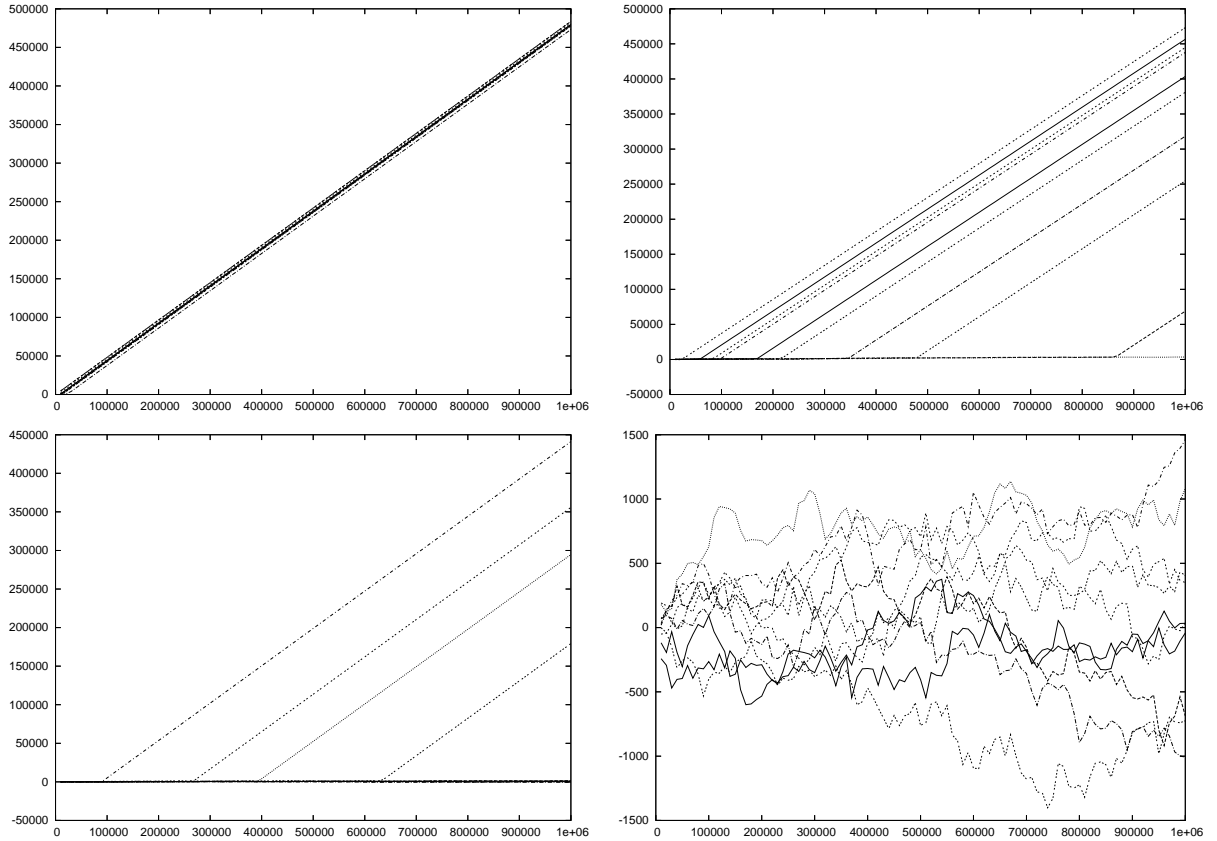


FIG. 13: Displacement versus time for ten trajectories for the parallel $\Delta y/\Delta x = 2$ system, for (a) $\epsilon = 0.1$, (b) $\epsilon = 0.01$, (c) $\epsilon = 10^{-3}$, and (d) $\epsilon = 10^{-4}$.

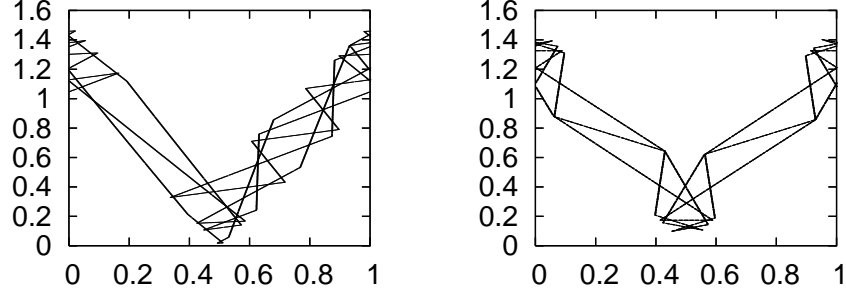


FIG. 14: Two distinct periodic trajectories of the finite field transport for the parallel $\Delta y/\Delta x = 2$ system for $\epsilon = 0.01$. The left hand side orbit has period $\tau = 12.393386...$ time units with 39 reflections per orbit. The right hand side orbit has period $\tau = 9.6950889...$ time units with 33 reflections per orbit.

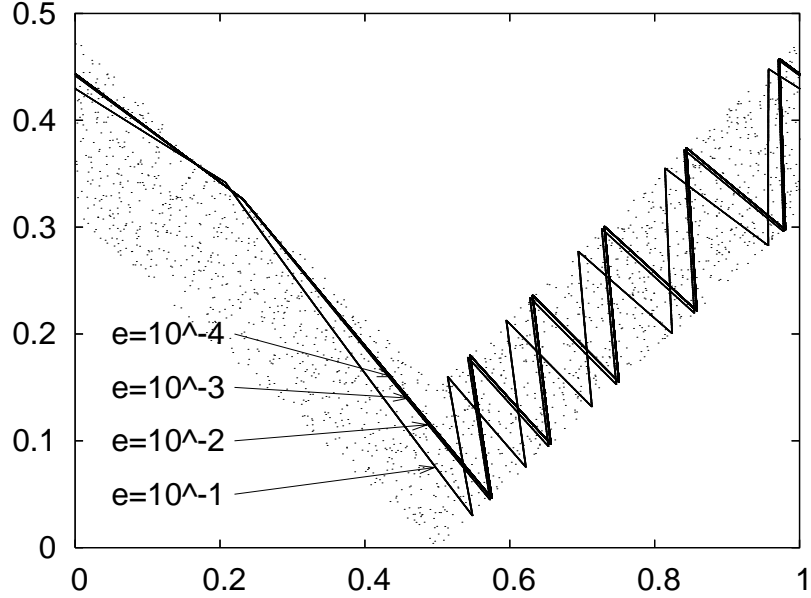


FIG. 15: (Attractive) periodic trajectories of the finite field transport for the $\Delta y_t/\Delta x = 0.62, \Delta y_b/\Delta x = 0.65, d = d_c$ system, for $0.1 < \epsilon < 10^{-4}$. The trajectories for the two weakest fields are indistinguishable on the scale of the figure. Cloud shown for aesthetic reasons.

Tables

$\Delta y/\Delta x$	saw-tooth systems					saw-tooth/flat systems		
	$0.5\Delta y$	$1.0\Delta y$	$1.05\Delta y$	$2.0\Delta y$	$20\Delta y$	$0.55\Delta y_t$	$2.0\Delta y_t$	$20\Delta y_t$
0.25	1.85	1.83	1.82	1.85	1.85	1.88	1.83	1.85
1	1.66	1.64	1.62	1.67	1.68	1.65	1.65	1.65
2	1.83	1.85	1.82	1.80	1.79	1.83	1.82	1.75
3	1.86	1.87	1.84	1.80	1.70	1.82	1.76	1.70

TABLE I: Equilibrium transport exponents: For saw-tooth boundary base triangles with height-width ratio $\Delta y/\Delta x$. For each (mean) pore height tested, the observed exponent out to 10^6 time units (of the order of 10^6 – 10^7 collisions) is given. The number of initial conditions used to compute averages ranges from 1000 to 5000, and the errors are estimated by ± 0.03 in all cases.

$\Delta y_t/\Delta x$	$\Delta y_b/\Delta x$	saw-tooth systems				
		$0.5\Delta y$	$1.0\Delta y$	$1.05\Delta y$	$2.0\Delta y$	$20\Delta y$
0.62	0.63	1.00(2)	1.02(2)	0.97(3)	1.03(7)	0.72(3)
0.62	0.64	1.00(1)	1.2(1)	1.03(3)	1.19(7)	1.10(5)
0.62	0.65	0.99(2)	1.02(2)	1.02(3)	0.97(6)	1.13(5)

TABLE II: Equilibrium transport exponents: For unparallel saw-tooth boundary base triangles with height-width ratio $\Delta y/\Delta x$. For each (mean) pore height tested, the observed exponent out to 10^6 time units (of the order of 10^6 – 10^7 collisions) is given. The number of initial conditions used to compute averages varies from 2000 up to 10^4 . Numbers in brackets correspond to error estimates from Marquardt-Levenberg least-squares fits.

field strength ϵ	parallel system	parallel system	unparallel system	unparallel system
	(raw)	(corrected)	(raw)	(corrected)
0.1	0.0935 ± 0.0001	0.0935 ± 0.0001	2.390 ± 0.003	2.390 ± 0.003
0.01	9.75 ± 0.2	0.205 ± 0.008	18.3 ± 0.2	0.24 ± 0.04
0.001	0.57 ± 0.04	0.57 ± 0.04	11 ± 1	0.19 ± 0.02
0.0001	0.28 ± 0.4	0.28 ± 0.4	1.2 ± 1	0.28 ± 0.14

equilibrium	∞	∞	0.386 ± 0.05	0.386 ± 0.05
-------------	----------	----------	------------------	------------------

TABLE III: Best estimates of the finite field diffusion coefficient $D(\epsilon)$ for $0.1 < \epsilon < 10^{-4}$ for the parallel $\Delta y/\Delta x = 2$ system, and the unparallel $\Delta y_t/\Delta x = 0.62, \Delta y_b/\Delta x = 0.65, d = d_c$ system, showing the raw data and data corrected for periodic orbits. Also included, for comparison, are the equilibrium results for the parallel case (exhibiting super-diffusive behaviour) and the unparallel case. Data was collected over 10^6 time units.

$\Delta y_t/\Delta x$	$\Delta y_b/\Delta x$	γ	$\Delta y_t/\Delta x$	$\Delta y_b/\Delta x$	γ
1	1.01	0.71(4)	2	2.02	1.04(2)
1	1.001	0.35(6)	2	2.002	1.01(2)
1	1.0001	0.66(5)	2	2.0002	1.04(2)
1	1.00001	0.58(3)	2	2.00002	1.02(2)
1	1.000001	0.53(5)	2	2.000002	0.98(2)
1	1	1.66(3)	2	2	1.83(3)

TABLE IV: Transport law exponent γ , as identified by (20), observed for various choices of $\Delta y_t/\Delta x$ and $\Delta y_b/\Delta x$. There appears to be no trend toward super-diffusive transport, arbitrarily close to (but away from) the parallel case. Numbers in brackets indicate errors in the last figure.